Submitted to Structural Safety (revised version) – December 2020

Variance of the fatigue damage in non-Gaussian stochastic processes with narrow-band power spectrum

Julian Marcell Enzveiler Marques*, Denis Benasciutti

Department of Engineering, University of Ferrara, via Saragat 1, 44122, Ferrara, Italy

ABSTRACT

This paper presents two theoretical models to assess the variance of the fatigue damage in stationary narrow-band and non-Gaussian stochastic processes. The models extend two solutions existing in the literature and restricted to Gaussian processes. The new models here developed exploit a non-linear transformation that links Gaussian and non-Gaussian domains based on skewness and kurtosis coefficients, which are used to quantify the deviation from the Gaussian distribution. Monte Carlo numerical simulations in time-domain are performed to confirm the correctness of the proposed non-Gaussian models, and to investigate the sensitivity of the variance of the damage to the skewness, kurtosis, and inverse slope of the stress versus life (S-N) curve. An example is finally presented to demonstrate the increase of the failure probability due to non-Gaussian effects in the stochastic loading.

Keywords: variance of fatigue damage; stochastic loadings; non-Gaussian; kurtosis; skewness; failure probability

Nomenclature

$\hat{C}_D$	sample coefficient of variation of damage
C_D	coefficient of variation of damage
d	fatigue damage of a half-cycle
$\overline{D}$	sample mean of fatigue damage
$D(T)$	fatigue damage in time period T
$E[d]^2$	expected damage squared
$E[d^2]$	expected value of damage squared
$f_a(s)$	probability distribution of stress amplitudes
$f_{P_0,P_l}(-)$	joint probability density function of two peaks
$G(-)$, $g(-)$	direct and inverse transformation
k, A	material constants of the stress-life (S-N) curve
$n(T)$, n	number of half-cycles counted in T
N_f	number of cycles to failure
$R_{\mathrm{X}}(\tau)$	autocorrelation function of $X(t)$
$R_{d_0,d_l}(l)$	autocorrelation function of half-cycle damage
s	stress amplitude of a half-cycle
$S_X(f)$, $S_Z(f)$	Power Spectral Density of $X(t)$ and $Z(t)$
(x_p, x_v), (z_p, z_v)	peak and valley (Gaussian, non-Gaussian)
$x(t)$, $z(t)$	Gaussian and non-Gaussian time-history
$X(t)$, $Z(t)$	Gaussian and non-Gaussian process
γ_3, γ_4	skewness, kurtosis
λ_m	m-th spectral moment
μ_X, μ_Z	mean value of $X(t)$ and $Z(t)$
ν_0	frequency of upward mean zero
$\rho_X(\tau)$, $\rho_Z(\tau)$	autocorrelation coefficient of $X(t)$ and $Z(t)$
$\rho_{d_0,d_l}(l)$	autocorrelation coefficient of half-cycle damage
$\hat{\sigma}_D^2$	sample variance of fatigue damage
σ_D^2	variance of fatigue damage
σ_X^2, σ_Z^2	variance of $X(t)$ and $Z(t)$
y^G, y^{nG}	(superscript) Gaussian, non-Gaussian
CoV	coefficient of variation

1 INTRODUCTION

Engineering structures and components are usually subjected to stochastic loadings during their service life. Examples are the loadings from road irregularity, wind or sea waves [1]. In practice, engineers estimate the probability of failure of such structures and components by calculating the damage values of measured time-history records, by means of the rainflow counting method and the Palmgren-Miner rule.

Stochastic time-history records have a random number of counted cycles, as well as randomly distributed amplitudes and mean values. Fatigue cycles and the damage computed therefrom are thus random variables, too. This means, for example, that the damage values computed from distinct stationary time-history records are not identical, even if the records are measured under nominally identical conditions and thus share the same statistical properties.

When only a limited number of time-history records of short time length are analysed, the information on the cycle distribution is not complete; as a result, the calculated damage values may represent a biased estimate of the "true" (or average) damage characterising a much larger set of time-histories. In other words, few damage values may have so large levels of statistical variability to make a fatigue life estimation rather uncertain (which, in turn, requires high safety factors to be introduced). The statistical variability (variance) of the damage is thus an essential property of the damage distribution, like as the mean value.

The attention on the estimation of the variance of fatigue damage dates from the sixties, when Mark and Crandall [2] and Bendat [3] proposed the first theoretical approaches. Their methods were, however, limited to the linear oscillator response (narrow-band Gaussian process). Subsequently, Madsen et al. [4] and Low [5] developed more general methods for estimating the variance of damage in narrow-band stochastic processes. Although not restricted to the linear oscillator, such methods apply to Gaussian processes only.

The hypothesis of Gaussian process is, however, not often satisfied by the stochastic loadings acting on real engineering structures. A loading that deviates from the Gaussian distribution is called non-Gaussian. The deviation is quantified by the skewness and kurtosis coefficients; the skewness measures the symmetry and the kurtosis the tail contribution in the probability distribution of a non-Gaussian process.

Non-Gaussian loadings are encountered, for example, in certain types of wind or wave loadings, or when the structure has a non-linear behaviour that transforms a Gaussian input into a non-Gaussian output [1]. One interesting situation is that of offshore structures subjected to wave stochastic loadings, in which structural nonlinearity combines with non-Gaussian input excitation.

These examples emphasised that the study of non-Gaussian stochastic loadings is of particular relevance in structural durability. In spite of this, at present there are no analytical approaches able to assess the variance of fatigue damage in non-Gaussian loadings. Apart from some exceptions [6], the methods existing in the literature are indeed valid for Gaussian loadings only.

This paper aims to present two theoretical models for estimating the variance of the damage in stationary non-Gaussian and narrow-band stochastic processes. The presented models extend two methods (Madsen et al. and Low) developed for Gaussian narrow-band processes. The models proposed in this paper are based on a time-invariant non-linear transformation that links a non-Gaussian stochastic process to its underlying Gaussian one. The transformation is calibrated on the values of skewness and kurtosis of the non-Gaussian process. The transformation permits the proposed models to estimate the variance for any combination of skewness and kurtosis coefficients.

The correctness of the proposed theoretical models is verified by Monte Carlo simulations, considering a linear oscillator response spectrum and an ideal unimodal power spectral density. Time-domain results from simulated time-histories (rainflow cycle counting and Palmgren-Miner

damage rule) are compared with theoretical estimations from the non-Gaussian models. The variance of the fatigue damage from non-Gaussian time-histories with different combinations of skewness and kurtosis is evaluated. Moreover, the paper investigates the relationship between the coefficient of variation in the Gaussian and non-Gaussian case as a function of both the distribution parameters (skewness and kurtosis) and the inverse slope of the stress versus life (S-N) curve. The unimodal power spectra density also permits different spectral bandwidths (from very narrow to mildly wide band) to be obtained and then used for scrutinising the actual range of validity of the proposed theoretical solutions when a power spectral density is not very narrow-band.

Finally, an example of structural integrity assessment is presented, which considers a structure subjected to both Gaussian and non-Gaussian stochastic loadings with same variance. The example is used to demonstrate the increase of failure probability due to the non-Gaussian characteristic of the stochastic loading.

The paper is organised as follows. Section 2 gives a short theoretical background on stochastic processes. Section 3 summarises the relevant formulas for the expected damage and variance, which have general validity. Section 4 reviews the Madsen et al.'s and Low's methods for the Gaussian case with the aim to summarise the main equations used later on by the two models extended to the non-Gaussian case. Section 5 introduces the non-linear transformation, then it develops the two proposed non-Gaussian models. They are implemented in Section 6, which verifies their correctness by Monte Carlo numerical simulations. Section 7 develops an example of structural integrity assessment to compare the failure probability for a structure subjected to stochastic loading either Gaussian or non-Gaussian. Finally, Section 8 summarises the main findings.

2 PROPERTIES OF STOCHASTIC PROCESSES

Let $X(t)$, $-\infty < t < \infty$ be a stationary Gaussian stochastic process. It represents an infinite ensemble of time-histories, $x_i(t)$, $i = 1,..,\infty$. The autocorrelation function of the process is $R_X(\tau) = E[X(t)X(t+\tau)]$, where symbol $E[-]$ is the probabilistic expectation and τ the time lag. The autocorrelation coefficient of $X(t)$ is [7]:

$$\rho_X(\tau) = \frac{R_X(\tau) - \mu_X^2}{\sigma_X^2} \tag{1}$$

which is bounded as $-1 \leq \rho_X(\tau) \leq 1$. In the formula, μ_X is the mean value and σ_X^2 the variance of the process. Both parameters μ_X and σ_X^2 define the normal probability distribution followed by the instantaneous values of the Gaussian process $X(t)$. Without loss of generality, it is assumed that $\mu_X = 0$.

The stochastic process $X(t)$ can also be described in the frequency-domain by a one-sided Power Spectral Density (PSD) $S_X(f)$, which is the Fourier transform of the autocorrelation function (Wiener-Khinchine relations) [7]:

$$S_X(f) = 4\int_0^\infty R_X(\tau)\, cos(2\pi f\tau)\, d\tau \qquad R_X(\tau) = \int_0^\infty S_X(f)\, cos(2\pi f\tau)\, df \tag{2}$$

The spectral moments $S_X(f)$ are [8]:

$$\lambda_m = \int_0^\infty (2\pi f)^m\, S_X(f)\, df, \quad m = 0,1,2\ldots \tag{3}$$

The variance of $X(t)$ is $\lambda_0 = R_X(0) = \sigma_X^2$, while the expected frequency of upward crossings of the mean value is $\nu_0^G = \sqrt{\lambda_2/\lambda_0}\,/2\pi$.

The Gaussian stochastic process $X(t)$ is fully determined by its expected value μ_X and by either its autocorrelation function $R_X(\tau)$ or, equivalently, its power spectrum $S_X(f)$.

Let $Z(t)$ be a stationary non-Gaussian stochastic process, with mean value μ_Z, variance σ_Z^2 and autocorrelation function $R_Z(\tau) = E[Z(t)Z(t+\tau)]$. As for $X(t)$, the autocorrelation coefficient

is also defined as $\rho_Z(\tau) = (R_Z(\tau) - \mu_Z^2)/\sigma_Z^2$. To simplify matter, it is assumed $\mu_Z = 0$. Similarly to Eq. (2), the power spectral density $S_Z(f)$ of the process is the Fourier transform of $R_Z(\tau)$. The expected frequency of upward crossings of the mean value is ν_0^{nG}.

Since the process $Z(t)$ is non-Gaussian, its instantaneous values do not follow a Gaussian probability distribution, but rather a non-normal probability distribution, whose degree of deviation from the normal distribution is usually quantified by the skewness, γ_3, and kurtosis, γ_4 [8]:

$$\gamma_3 = \frac{E[(Z(t) - \mu_Z)^3]}{\sigma_Z^3} \qquad \gamma_4 = \frac{E[(Z(t) - \mu_Z)^4]}{\sigma_Z^4} \tag{4}$$

which are the standardised third and fourth central moments, respectively. The skewness measures the asymmetry degree of a non-Gaussian distribution. The kurtosis measures the contribution of the tails of the distribution: values away from the mean can be either higher ($\gamma_4 > 3$, leptokurtic case) or lower ($\gamma_4 < 3$, platykurtic case) than the values of a Gaussian distribution. A Gaussian process has $\gamma_3 = 0$ and $\gamma_4 = 3$.

In this way, the probability law of the non-Gaussian process $Z(t)$ is fully specified by four statistical parameters (μ_Z, σ_Z^2, γ_3, γ_4), rather than by the entire non-normal probability distribution. Note that γ_3 and γ_4 provide a sufficiently accurate description of a mildly non-normal behavior ([9,10]). More refined approximations of the non-normal probability distribution of $Z(t)$ would involve higher order central moments $E[Z^n(t)]$, which would nevertheless be more sensitive to the sampling variability when estimated from observed data.

The non-Gaussian stochastic process $Z(t)$ is completely determined by its expected value μ_Z, skewness γ_3, kurtosis γ_4, and by either its autocorrelation function $R_Z(\tau)$ or, equivalently, its power spectrum $S_Z(f)$.

It should be stressed that no "physical" relationship exists between the two processes $X(t)$ and $Z(t)$ introduced so far. That is, they do not represent the input and output of a mechanical system. Rather, both processes may represent the output (e.g. load, stress or strain) acting at the

135 critical location in a system or structure. For example, $X(t)$ may represent the Gaussian output of a linear system driven by a Gaussian input, whereas $Z(t)$ could be the non-Gaussian output in case the system behaves nonlinearly. In this circumstance, the probabilistic properties of $X(t)$ and $Z(t)$ are not related to each other.

Instead, in Section 5.1 the two processes will be linked via a memoryless transformation. 140 Only in this case (and only this) $X(t)$ does not represent any physical quantity (load or stress), but rather it must be viewed as a sort of hidden Gaussian process underlying $Z(t)$. The transformation is introduced as a mathematical tool that allows the results on the damage (expected value, variance and coefficient of variation) to be extended from the Gaussian to the non-Gaussian case. The transformation is calibrated based on the statistical properties of $Z(t)$.

145 On the other hand, it should be mentioned that in some engineering applications – not considered here – the two processes represent the non-Gaussian output $Z(t)$ of a nonlinear mechanical system driven by a Gaussian input $X(t)$. In this case, the memoryless transformation is used to describe the nonlinear feature of the system and it allows the statistical properties of the output $Z(t)$ to be computed analytically from those of the input $X(t)$ (see [11,12,13] and the 150 Winterstein's model in Appendix A). This kind of input/output relationship will not be considered in the following.

3 EXPECTED VALUE AND VARIANCE OF DAMAGE: THEORETICAL BACKGROUND

3.1 EXPECTED VALUE OF DAMAGE

Assume that $x(t)$, $0 < t < T$, represents a time-history of time duration T from the stochastic 155 process $X(t)$. The fatigue damage under the Palmgren-Miner rule is:

$$D(T) = \sum_{i=0}^{n(T)-1} d_i = \sum_{i=0}^{n(T)-1} \frac{s_i^k}{2A} \tag{5}$$

in which s_i is the stress amplitude of the i-th half-cycle, $n(T)$ indicates the number of half-cycles counted in T, A and k are material constants of the S–N curve $s^k N_f = A$, where N_f is the number of cycles to failure at constant amplitude s. More specifically, the strength constant $A = s_A^k N_{f,A}$ is computed from the strength amplitude s_A corresponding to the number of cycles $N_{f,A}$ (typically $2 \cdot 10^6$ cycles). The values of k and A (or s_A) follow from a regression analysis of experimental fatigue data on identical specimens; the regression line refers to a failure probability of 50%. A statistical analysis of fatigue data can account for the uncertainty of the estimates and the inherent scatter of experimental data, and it allows a characteristic S-N curve to be defined in which s_A refers to a prescribed failure probability, e.g. 2.5% [14].

The damage $D(T)$ is a random variable as it depends on the specific time-history $x(t)$ of time length T. Indeed, it takes on different values from one time-history to another due to the randomness in stress amplitudes and number of half-cycles counted in T.

The expected damage is derived by taking the expectation of Eq. (5):

$$E[D(T)] = E\left[\sum_{i=0}^{n(T)-1} d_i\right] = E[n(T)]\frac{E[s^k]}{2A} \tag{6}$$

Equation (6) represents the damage of the whole ensemble of time-histories of $X(t)$, i.e. it represents the damage of $X(t)$. The quantity $E[n(T)]$ is the expected number of half-cycles counted in T, whereas $E[d] = E[s^k]/2A$ denotes the expected damage per half-cycle. The term $E[d]$ is the k-th moment of the probability distribution of stress amplitudes $f_a(s)$:

$$E[d] = \frac{1}{2A}\int_0^\infty s^k f_a(s)\, ds \tag{7}$$

In a narrow-band process, the stress amplitude distribution $f_a(s)$ equals the peak distribution; if the process is also Gaussian, the peak distribution is Rayleigh. The resulting expected damage per half-cycle is [15]:

$$E[d^G] = \frac{1}{2A}\left(\sqrt{2\lambda_0}\right)^k \Gamma\left(1+\frac{k}{2}\right) \tag{8}$$

where $\Gamma(-)$ is the gamma function.

For a narrow-band process, the expected number of counted half-cycles is $E[n(T)] = 2\nu_0 T$. Using the relationship $E[D^G(T)] = 2\nu_0^G T \cdot E[d^G]$, the expected damage for a narrow-band Gaussian process then becomes:

$$E[D^G(T)] = \frac{\nu_0^G T}{A}\left(\sqrt{2\lambda_0}\right)^k \Gamma\left(1+\frac{k}{2}\right) \tag{9}$$

3.2 VARIANCE OF DAMAGE

Under the assumption of stationary damage process and deterministic number of half-cycles $n(T) = 2\nu_0 T$, the general expression of the variance of damage (omitting T from symbol n) is [2]:

$$\sigma_D^2 = n(E[d_0^2] - E[d_0]^2) + 2\sum_{l=1}^{n-1}(n-l)(E[d_0 d_l] - E[d_0]^2) \tag{10}$$

where l is a time lag that takes on integer values from 1 to $n-1$. Note that $E[d_0^2]$ denotes the "expected value of the damage squared", whereas $E[d_0]^2$ denotes the "expected damage squared".

In the previous expression, the time lag l is related to the time difference $\tau = l/(2\nu_0)$ between two peaks, P_0 and P_l ("peak" is applied in a broad sense to indicate both peaks and valleys, see [5]). Furthermore, the damage per half-cycle d_l is proportional to P_l^k. Accordingly, the product $E[d_0 d_l]$ can be computed from the joint probability density function (JPDF) of two peaks, $f_{P_0,P_l}(x_p, x_v)$ as:

$$E[d_0 d_l] = \frac{1}{4A^2}\iint_{-\infty}^{\infty} x_p^k x_v^k \, f_{P_0,P_l}(x_p, x_v)\,\mathrm{d}x_p\,\mathrm{d}x_v \tag{11}$$

This equation defines the autocorrelation function of half-cycle damage, $R_{d_0,d_l}(l) = E[d_0 d_l]$. In analogy with Eq. (1), the autocorrelation coefficient of half-cycle damage is introduced:

$$\rho_{d_0,d_l}(l) = \frac{R_{d_0,d_l}(l) - \mu_d^2}{\sigma_d^2} \tag{12}$$

which is bounded as $0 \leq \rho_{d_0,d_l}(l) \leq 1$.

It is possible to demonstrate that Eq. (10) can also be written as a function of $\rho_{d_0,d_l}(l)$ [5]:

$$\sigma_D^2 = \left[n + 2\sum_{l=1}^{n-1}(n-l)\rho_{d_0,d_l}(l)\right](E[d_0^2] - E[d_0]^2) \tag{13}$$

A general closed-form equation for the variance σ_D^2 is not available unless some hypothesis (Gaussian process) is introduced, as in the two models that are reviewed in the next Section.

4 GAUSSIAN MODELS

This section presents a brief account of two models for estimating the variance of damage in a narrow-band Gaussian process. These models are the basis from which the non-Gaussian models, described in later sections, are developed.

4.1 LOW'S METHOD

Low derived a best-fitting equation of $\rho_{d_0,d_l}^G(l)$ by solving the product expectation in Eq. (11) through the use of the Rice JDPF of peaks and valleys for a narrow-band process [16]:

$$f_{P_0,P_l}^G(x_p, x_v) = \frac{x_p x_v}{1 - \rho_X^2(l)} I_0\left(\frac{x_p x_v\, \rho_X(l)}{1 - \rho_X^2(l)}\right) e^{-\frac{x_p^2 + x_v^2}{2\left(1-\rho_X^2(l)\right)}} \tag{14}$$

in which $I_0(-)$ is the modified Bessel function of the first kind with order zero. This distribution comes from the definition of the envelope process, based on the concept of auxiliary process [5].

By using a symbolic computation software, the double integral in Eq. (11) was solved in closed form for $k = 2$, 4 and 6 [5]:

$$\rho^{G}_{d_0,d_l}(l) = \begin{cases} \rho^2_X(l) & \text{for } k = 2 \\ \frac{4}{5}\rho^2_X(l) + \frac{1}{5}\rho^4_X(l) & \text{for } k = 4 \\ \frac{1}{19}\left(9\rho^2_X(l) + 9\rho^4_X(l) + \rho^6_X(l)\right) & \text{for } k = 6 \end{cases} \quad (15)$$

(due to a misprint, in [5] the coefficients of the second equation are switched).

Afterward, the autocorrelation coefficient $\rho^{G}_{d_0,d_l}(l)$ was approximated by a quadratic interpolation function of $\rho^2_X(l)$ as $\rho^{G}_{d_0,d_l}(l) = \alpha_k \rho^2_X(l) + \beta_k \rho^4_X(l)$, where α_k and β_k are best-fitting coefficients that depend upon k (their values are tabulated in [5]). The fitting was restricted to integer values in the range $1 \leq k \leq 9$. With this approximation and by invoking Eq. (8) and Eq. (13), the variance of fatigue damage turns into:

$$(\sigma^2_D)^{G}_{\text{Low}} = \left\{ n + 2\sum_{l=1}^{n-1} (n-l)\left(\alpha_k \rho^2_X(l) + \beta_k \rho^4_X(l)\right) \right\} \frac{(2\lambda_0)^k}{4A^2} \left[\Gamma(1+k) - \Gamma^2\left(1 + \frac{k}{2}\right) \right] \quad (16)$$

The square root of the ratio of the variance σ^2_D to the expected damage value squared $E[D(T)]^2$ defines the coefficient of variation (CoV) of the damage:

$$(C_D)^{G}_{\text{Low}} = \frac{1}{n} \sqrt{ \left\{ n + 2\sum_{l=1}^{n-1} (n-l)\left(\alpha_k \rho^2_X(l) + \beta_k \rho^4_X(l)\right) \right\} \left[\frac{\Gamma(1+k)}{\Gamma^2\left(1 + \frac{k}{2}\right)} - 1 \right] } \quad (17)$$

To apply the Low's method one only needs to know the autocorrelation function $R_X(\tau)$ of the Gaussian process $X(t)$, the fitting constants α_k, β_k that are tabulated in [5], and the S-N parameters A, k for the material or structural detail (actually, A is only required to compute the variance in Eq. (16)). Other quantities in Eq. (16)-(17) can be obtained readily. For example, $\rho_X(\tau)$ comes directly from $R_X(\tau)$, whereas the number of half-cycles can be estimated by the average $n = 2\nu^G_0 T$ that depends on the mean upcrossing frequency $\nu^G_0 = \sqrt{\lambda_2/\lambda_0}\,/2\pi$, computed from the spectral moments of the power spectrum $S_X(f)$ of $X(t)$. On the other hand, $S_X(f)$ can be obtained from $R_X(\tau)$, see Eq. (2). If $R_X(\tau)$ or $S_X(f)$ are not known exactly by a mathematical expression, they can be estimated from a time-history sample $x(t)$, although this introduces a sampling error [17].

4.2 MADSEN ET AL.'S METHOD

This method considers the autocorrelation coefficient $\rho^G_{d_0,d_l}(l)$ computed from the envelope of a narrow-band process [18]. For a S-N slope $k = 2$, the autocorrelation coefficient of the damage is approximated in [4] as:

$$\rho^G_{d_0,d_l}(l) \cong \rho^2_X(l) + \left(\frac{\rho'_X(l)}{2\pi\nu^G_0}\right)^2 \tag{18}$$

where $\rho_X(l)$ is the autocorrelation coefficient and $\rho'_X(l)$ its first derivative with respect to τ, both functions computed at the time lag $\tau = l/(2\nu^G_0)$.

Compared to Eq. (15) for $k = 2$, the expression of $\rho^G_{d_0,d_l}(l)$ now includes a first derivative term. This difference lies in which definition of the envelope is adopted [19]: Cramer-Leadbetter envelope from the analytic signal in [5], Crandall-Mark envelope from the derivative process in [4].

By inserting Eq. (18) and Eq. (8) into Eq. (13), the variance for $k = 2$ is computed as:

$$(\sigma^2_D)^G_{\mathrm{Mad}} = \left\{n + 2\sum_{l=1}^{n-1}(n-l)\left[\rho^2_X(l) + \left(\frac{\rho'_X(l)}{2\pi\nu^G_0}\right)^2\right]\right\}\frac{(2\lambda_0)^k}{4A^2}\left[\Gamma(1+k) - \Gamma^2\left(1+\frac{k}{2}\right)\right] \tag{19}$$

Eq. (19) consists of a summation of terms related to the autocorrelation coefficient $\rho_{\mathrm{X}}(l)$. The expression of the CoV is:

$$(C_D)^G_{\mathrm{Mad}} = \frac{1}{n}\sqrt{\left\{n + 2\sum_{l=1}^{n-1}(n-l)\left[\rho^2_X(l) + \left(\frac{\rho'_X(l)}{2\pi\nu^G_0}\right)^2\right]\right\}\left[\frac{\Gamma(1+k)}{\Gamma^2\left(1+\frac{k}{2}\right)} - 1\right]} \tag{20}$$

Equations (19) and (20) are valid for any narrow-band Gaussian process. Note the close similarity between these two last expressions and the formulas (16) and (17); the only difference lies in the definition of the autocorrelation coefficient of damage.

It must however be remarked that in Ref. [20] the range of validity of Eq. (18), and therefore of Eqs. (19)-(20), was incorrectly extended to values of k other than two. This is a mistake. For even values of k, the correct expressions of $\rho^G_{d_0,d_l}(l)$ for are those of Low [5], and reported in Eq. (15). Such expressions holds true also for the Madsen et al.'s method, provided that $\rho^2_X(l)$ on the right hand side of Eq. (15) is replaced with $\rho^2_X(l) + \left(\frac{\rho'_X(l)}{2\pi\nu^G_0}\right)^2$.

Surprisingly, the above-mentioned mistaken formulas were observed to agree quite well with numerical simulations, see Ref. [20] and Section 6 later. This unexpected result suggests that the use the above formulas for any $k \neq 2$ constitutes a theoretically incorrect but nevertheless acceptable approximation in that it does not introduce relevant errors in the estimation. This conclusion can be explained by the role of $\rho^{\mathrm{G}}_{\mathrm{d_0,d_l}}(l)$ in the summation in Eqs. (19)-(20), along with the trends of Figure 1. The figure compares Eq. (18) with the autocorrelation of the damage computed from simulations, for values $k = 2, 4, 6$. The lower frame displays the ratio of the theoretical to simulated values of $\rho^G_{d_0,d_l}(l)$. The results come from a Monte Carlo study with a unimodal PSD, for a total of $8 \cdot 10^5$ simulated time-history realisations.

As expected, for $k = 2$ the formula in Eq. (18) works well, whereas for other k an error is introduced. It is seen that, as the time lag l increases, the error increases but the values of $\rho^G_{d_0,d_l}(l)$ become increasingly small. These two opposite trends compensate each other. This net effect is explained by considering that in Eqs. (19) and (20) the quantity $(n-l)\rho^G_{d_0,d_l}(l)$ is summed up at increasing time lags l, from 1 to $n-1$. At small indexes l, the quantity $(n-l)\rho^G_{d_0,d_l}(l)$ is almost exact and contributes much to the entire sum, whereas at larger indexes l where the error increases its contribution becomes increasingly negligible. As a result, Eq. (18) provides a satisfactory estimation accuracy for any k.

Please insert here Figure 1

As a final note, to apply the Madsen et al.'s method one only needs to know the autocorrelation function $R_X(\tau)$ of the Gaussian process $X(t)$ and the S-N parameters. Other quantities can be obtained readily, as previously explained for the Low's method.

5 NON-GAUSSIAN MODELS

A convenient way to represent a non-Gaussian stochastic process is by means of a translation model. In this model, a non-Gaussian process $Z(t)$ is mapped from an underlying Gaussian process $X(t)$ by the use of a time-independent non-linear transformation $G(-)$ [11,12,13]. The functional form of the transformation is established by the mapping $G(-) = F_Z^{-1}\{F_X[-]\}$ between the cumulative distribution functions, $F_X(-)$ and $F_Z(-)$, of the Gaussian and the non-Gaussian process, respectively. The transformation so defined assures that the values of the non-Gaussian process match the probability distribution $F_Z(-)$, chosen arbitrarily. The transformation also allows the main statistical properties (mean, variance and autocorrelation function) of the non-Gaussian process to be calculated from those of the underlying Gaussian process [11].

In this article, the transformation $G(-)$ is used for including the non-Gaussian effects into the previous two Gaussian models for the variance of the damage.

5.1 DEFINITION OF THE TRANSFORMATION

The transformation $G(-)$ establishes a one-to-one relationship between the values of Gaussian and non-Gaussian processes. The non-Gaussian process is thus obtained as $Z(t) = G(X(t))$. Conversely, the Gaussian process $X(t) = g(Z(t))$ is transformed back by the inverse function $g(-) = G^{-1}(-)$. The degree of non-linearity of the transformation is calibrated on the values of skewness γ_3 and kurtosis γ_4 characterising the non-Gaussian process (usually, $\gamma_3 \neq 0$ and $\gamma_4 \neq 3$). If $\gamma_3 = 0$ and $\gamma_4 = 3$, the process $Z(t)$ becomes Gaussian and the transformation linear. Note that

the transformation must be monotonically increasing in order to obtain a non-Gaussian process correctly. The transformation is independent of t.

Please insert here Figure 2

Various forms of either the direct or the inverse transformation are available in the literature: Ochi's model is a monotonic exponential function [21], Winterstein's model is based on cubic Hermite polynomials [9,22,23], whereas the transformation of Sarkani et al. makes use of a power law model [24,25]. Among them, only the Winterstein's model provides the analytical expressions of both the direct and the inverse transformations, $G(-)$ and $g(-)$, see Appendix A. This aspect turns out to be particularly advantageous in the development of the non-Gaussian solutions for the variance, presented in this Section. An example of linear and non-linear transformations is depicted in Figure 2(a), which shows the relationship between $X(t)$ and the transformed $Z(t) = G(X(t))$. The non-linear case is obtained by the Winterstein's model and refers to values $\gamma_3 = 0.5$ and $\gamma_4 = 6$.

For what follows, it is convenient to recall the expression of the autocorrelation coefficient of the non-Gaussian process [10,22]:

$$\rho_Z(\tau) = \kappa^2[\rho_X(\tau) + 2c_3^2\rho_X^2(\tau) + 6c_4^2\rho_X^3(\tau)] \tag{21}$$

in terms of the autocorrelation coefficient of the Gaussian process, $\rho_X(\tau)$. Coefficients κ and c_i are defined in Appendix A.

The previous formula shows that the translation model only makes the two autocorrelation functions differ by second-order terms in the coefficients κ, c_3, and c_4. By quoting Refs. [10,22], "the functional transformation can substantially alter the static distribution of a normal process without greatly changing its correlation structure." From a practical point of view, the difference between $\rho_Z(\tau)$ and $\rho_X(\tau)$ is almost negligible. This fact is confirmed by the example in Figure 3, which compares the autocorrelation coefficient of a band-limited Gaussian process to that of a

transformed non-Gaussian process. The Gaussian process has autocorrelation coefficient $\rho_X(\tau) = \cos(\omega_c \tau)\sin(b\tau)/(b\tau)$, where $\omega_c = 2\pi f_c$ is the central angular frequency (in rad/s) and b the half-bandwidth of the corresponding power spectral density depicted in Figure 5(b).

Figure 3 considers two bandwidths ($b = 1, 10$), and a non-Gaussian process with skewness $\gamma_3 = 0.5$ and kurtosis $\gamma_4 = 6$. Note that the results are suitably normalised so to be independent of the particular values of ω_c and b. The figure confirms that $|\rho_Z(\tau)| \leq |\rho_X(\tau)|$ (see [11]) and shows that the difference between $\rho_X(\tau)$ and $\rho_Z(\tau)$ reaches an absolute maximum of about 3%, while for $\gamma_4 = 8$ (which yet represents a rather high value) the difference increases up to 6% (not shown in the figure). The deviation is more sensitive to kurtosis than skewness, and it obviously decreases to zero when the kurtosis approaches 3 (Gaussian case). In summary, although a difference between $\rho_Z(\tau)$ and $\rho_X(\tau)$ exists, it was observed to be small for kurtosis values of practical interest; this suggests that the approximation $\rho_Z(\tau) \cong \rho_X(\tau)$ – adopted in the following sections – is rather acceptable.

It has finally to be mentioned that the transformation, especially if it has a high degree of non-linearity (e.g. high kurtosis value), may introduce some harmonic distortion on the power spectrum $S_Z(f)$ of the transformed process $Z(t)$ [26]. However, if the degree of non-linearity of $G(-)$ is not too high, the distortion is acceptable and both processes have similar spectral contents [26]. Similarly to the distortion effect mentioned for the autocorrelation function, also the "redistribution of power [in a PSD] is a second-order effect" [10,22], when compared with the changes in the probability distributions.

5.2 NON-GAUSSIAN SOLUTION BASED ON LOW'S METHOD

The Low's model for the variance of the damage in a Gaussian process is now extended to the non-Gaussian case. The Gaussian model is based on four properties of a narrow-band Gaussian process:

i) the expected number of half-cycles in time interval T is equal to the frequency of upward crossings, $E[n(T)] = 2\nu_0^G T$;

ii) the time lag between two peaks P_l^G and P_{l+1}^G is $\tau = l/\left(2\nu_0^G\right)$;

iii) the JPDF of two peaks $f_{P_0,P_l}^G(x_p, x_v)$ is the Rice distribution in Eq. (14), which is used to derive the autocorrelation coefficient of the damage $\rho_{d_0,d_l}^G(l)$;

iv) the probability distribution of peaks $f_{P_0}^G(x_p)$ is known to be a Rayleigh distribution.

The first and second conditions are, in fact, very general and hold true also for a narrow-band process that is non-Gaussian, as they only rely on the characteristics of a narrow-band process. The third and fourth conditions, instead, require the Gaussian hypothesis for the process.

A useful property of the non-linear transformations $G(-)$ and $g(-)$ is that to establish a one-to-one relationship between a value in a Gaussian process at any time instant and its transformed value in the non-Gaussian process, at the same time instant. This relationship ensures that peaks, valleys and mean value crossings are placed exactly at the same time instants in both processes. Figure 2(b) highlights this relationship for the peaks in the Gaussian and non-Gaussian process.

For example, if the Gaussian process crosses its mean value μ_X at time t_1, that is $X(t_1) = \mu_X$, the non-Gaussian process will cross its mean value μ_Z also at t_1, that is $Z(t_1) = \mu_Z$. Moreover, if $X(t)$ has a peak $x_p(t)$ or valley $x_v(t)$ at time instant t, the non-Gaussian process will have a corresponding peak or valley at the same time instant, $z_p(t) = G\left(x_p(t)\right)$ and $z_v(t) = G(x_v(t))$. The same condition holds true also for the inverse relationship $x_p(t) = g\left(z_p(t)\right)$ and $x_v(t) = g(z_v(t))$. In addition, the previous discussion emphasised that, from a practical point of view, the autocorrelation coefficient of the non-Gaussian process can be approximated as $\rho_Z(l) \cong \rho_X(l)$.

An additional and more important consequence is that the relative positions of peaks and valleys in both processes are preserved for a monotonic transformation. For example, two peaks will be $z_p(t_1) > z_p(t_2)$ in the non-Gaussian process if they are transformed by $G(-)$ from two

peaks $x_p(t_1) > x_p(t_2)$ at any time instants t_1, t_2 in the Gaussian process. Of course, the same concept applies to valleys as well. This is the same as saying that if the Gaussian process has peaks $P_l^G > P_{l+1}^G$ at time lag l, the non-Gaussian process will have peaks $P_l^{nG} > P_{l+1}^{nG}$ at the same time lag.

The previous insights may be synthesised by saying that a non-linear transformation from a Gaussian to a non-Gaussian process preserves the number of mean value crossings, and either increases or decreases (depending on γ_3, γ_4) the values of peaks and valleys, keeping their relative positions unaltered. This property, in particular, guarantees that, in the non-Gaussian process, half-cycles are formed by peak/valley pairs that are transformed from the corresponding peak/valley pairs in the Gaussian process, and that the non-Gaussian half-cycles have amplitudes smaller or larger (depending on γ_3, γ_4) than the corresponding amplitudes of the Gaussian half-cycles.

In light of the previous observations, the four properties summarised in the previous bulleted list can easily be adapted to the non-Gaussian case. More precisely, in a non-Gaussian narrow-band process:

i) the expected number of half-cycles in time interval T is equal to the frequency of upward crossings: $E[n(T)] = 2\nu_0^{nG}T$, where $\nu_0^{nG} = \nu_0^G$;

ii) the time lag between two peaks P_l^{nG} and P_{l+1}^{nG} is $\tau = l/(2\nu_0^{nG})$;

iii) the autocorrelation coefficient $\rho_{d_0,d_l}^{nG}(l)$ is derived from the JPDF $f_{P_0,P_l}^{nG}(z_p, z_v)$ of two peaks, which is obtained as a variable transformation of the Rice distribution in Eq. (14);

iv) the distribution of peaks for non-Gaussian $f_{P_0}^{nG}(z_p)$ is obtained by a variable transformation of the Rayleigh distribution valid in the Gaussian case;

The first two properties are obvious; the other two needs some explanation. The third condition is now elaborated further. Let us consider a pair of any two local extremes z_p and z_v (peak and valley) in the non-Gaussian process. They are random variables with joint probability density function, say $f_{P_0,P_l}^{nG}(z_p, z_v)$. Such local extremes are transformed back to two corresponding local extremes

$x_p = g(z_p)$ and $x_v = g(z_v)$ (peak and valley) in the Gaussian process through the inverse transformation $g(-)$. For the Gaussian local extremes is valid the joint Rice distribution in Eq. (14). It is therefore straightforward to derive the joint distribution of the non-Gaussian local extremes by the rule of transformed random variables [8]:

$$f^{nG}_{P_0,P_l}(z_p, z_v) = f^{G}_{P_0,P_l}(x_p, x_v) \cdot \left| \mathbf{J}(x_p, x_v) \right|^{-1} \tag{22}$$

where symbol $|-|$ denotes the absolute value and $\mathbf{J}$ is the Jacobian of the transformation $g(-)$, which turns out from the following 2×2 determinant:

$$\mathbf{J}(x_p, x_v) = \begin{vmatrix} \dfrac{\partial g(z_p)}{\partial z_p} & \dfrac{\partial g(z_p)}{\partial z_v} \\ \dfrac{\partial g(z_v)}{\partial z_p} & \dfrac{\partial g(z_v)}{\partial z_v} \end{vmatrix} \tag{23}$$

The inverse transformation must be applied to peak and valley variables separately. As a result, the Jacobian in Eq. (23) is, in fact, a diagonal matrix. Intuition suggests, for example, that an infinitesimal change in the non-Gaussian peak ∂z_p produces no variation in the corresponding valley ∂z_v, and therefore $\partial g(z_p)/\partial z_v = 0$. A similar reasoning applied to the other out-of-diagonal term explains why $\partial g(z_v)/\partial z_p = 0$.

By considering the Rice formula in Eq. (14), the general expression in Eq. (22) can be written more specifically as:

$$f^{nG}_{P_0,P_l}(z_p, z_v) = \frac{g(z_p)g(z_v)}{1-\rho_Z^2(l)} I_0\left(\frac{g(z_p)g(z_v)\,\rho_Z(l)}{1-\rho_Z^2(l)}\right) e^{-\frac{g(z_p)^2+g(z_v)^2}{2\left(1-\rho_Z^2(l)\right)}} \left| \frac{\partial g(z_p)}{\partial z_p} \cdot \frac{\partial g(z_v)}{\partial z_v} \right|^{-1} \tag{24}$$

Although not written explicitly, the Bessel function $I_0(z_p, z_v)$ in Eq. (24) is a function of z_p and z_v, and it is obtained by a simple change of variables in the corresponding function $I_0(x_p, x_v)$ in Eq. (14), which instead depends on the variables x_p and x_v.

The expression in Eq. (24) represents the joint distribution of two peaks in the non-Gaussian process $Z(t)$. As the transformation of variables involves the non-linear function $g(z_p)$ and its derivatives, the final expression is so complex that is not possible to arrive at a closed-form solution. A numerical approach must be used.

Eq. (24) depends on both γ_3 and γ_4 through function $g(z_p)$. It is also function of μ_Z, σ_Z^2 and ρ_Z. Obviously, in the limiting case $\gamma_3 = 0$ and $\gamma_4 = 3$ (Gaussian process), Eq. (24) converges to the Rice distribution in Eq. (14).

Figure 4(a) compares the Gaussian and non-Gaussian joint probability distributions of peaks (the latter obtained with $\mu_Z = 0$, $\sigma_Z^2 = 1$, $\rho_Z = 0$, $\gamma_3 = 0.5$ and $\gamma_4 = 6$). The distributions are plotted on the region of positive values pertaining to peaks. The shift of probabilities is clear. In particular, if compared to the Gaussian case, the non-Gaussian distribution shows higher levels of probability towards larger peak values.

Please insert here Figure 4

The non-Gaussian peak-peak joint distribution obtained so far allows the damage correlation $E[d_0^{nG} d_l^{nG}]$ to be computed with no much effort by solving numerically the double integral in Eq. (11). Attention must be paid in the numerical integration when the kurtosis γ_4 is very large. In this circumstance, indeed, the non-Gaussian variables z_p, z_v extend over a rather wide interval that needs to be finely discretised to assure the necessary numerical precision.

The last point iv) in the previous list for the non-Gaussian process is finally considered. In the same way as Eq. (22), the probability density function of peaks in the non-Gaussian process is determined by a variable transformation [8]:

$$f_{P_0}^{nG}(z_p) = f_{P_0}^{G}(x_p) \left| \frac{\partial g(z_p)}{\partial z_p} \right|^{-1} \tag{25}$$

Making use of Eq. (25) and introducing the transformed random variable $x_p = g(z_p)$ into the formula of the Rayleigh distribution $f_{P_0}^{G}(x_p)$, the probability distribution of peaks in the non-Gaussian case can be written as:

$$f_{P_0}^{nG}(z_p) = \frac{g(z_p)}{\sigma_Z^2}\, e^{-\frac{\left(g(z_p)\right)^2}{2\sigma_Z^2}} \left|\frac{\partial g(z_p)}{\partial z_p}\right|^{-1} \tag{26}$$

Equation (26) depends on the four statistics μ_Z, σ_Z^2, γ_3, γ_4 characterising the non-Gaussian process $Z(t)$. It converges to a Rayleigh distribution when $\gamma_3 = 0$ and $\gamma_4 = 3$ (Gaussian process).

A comparison of the Gaussian and the non-Gaussian (transformed) distribution is sketched in Figure 4(b). It refers to $\mu_Z = 0$, $\sigma_Z^2 = 1$, $\gamma_3 = 0.5$ and $\gamma_4 = 6$. The wider tail in the non-Gaussian distribution provides higher levels of probability towards larger peak values.

Similarly to Eq. (7), the expected value of the damage $E[d_0^{nG}]$ and its square $E[(d_0^{nG})^2]$ are nothing more than the moments of order k and $2k$, respectively, of the probability distribution $f_{P_0}^{nG}(z_p)$ just introduced. On substituting the non-Gaussian distribution in Eq. (26) into Eq. (7), the general expression that gives both expected damage values is:

$$E[(d_0^{nG})^q] = \frac{1}{(2A)^q} \int_0^{\infty} z_p^{q\cdot k}\, \frac{g(z_p)}{\sigma_Z^2}\, e^{-\frac{\left(g(z_p)\right)^2}{2\sigma_Z^2}} \left|\frac{\partial g(z_p)}{\partial z_p}\right|^{-1} \mathrm{d}z_\mathrm{p} \tag{27}$$

where the exponent q is 1 or 2. Note that this expression is only a function of μ_Z, σ_Z^2, γ_3, γ_4.

The variance of the fatigue damage for the non-Gaussian process is finally obtained through Eq. (10), in which the quantities $E[d_0^{nG} d_l^{nG}]$, $E[(d_0^2)^{nG}]$ and $E[d_0^{nG}]$ calculated so far for the non-Gaussian process have to be used:

$$(\sigma_D^2)_{\mathrm{Low}}^{nG} = n(E[(d_0^2)^{nG}] - E[d_0^{nG}]^2) + 2\sum_{l=1}^{n-1}(n-l)(E[d_0^{nG} d_l^{nG}] - E[d_0^{nG}]^2) \tag{28}$$

This expression extends the Low's method to the non-Gaussian case. Note that $E[(d_0^2)^{nG}]$ denotes the "expected value of the damage squared", whereas $E[d_0^{nG}]^2$ denotes the "expected damage squared".

The corresponding expression of the CoV for the non-Gaussian process becomes:

$$(C_D)_{\text{Low}}^{nG} = \frac{1}{n}\sqrt{n\left(\frac{E[(d_0^2)^{nG}]}{E[d_0^{nG}]^2} - 1\right) + \frac{2\sum_{l=1}^{n-1}(n-l)(E[d_0^{nG}d_l^{nG}] - E[d_0^{nG}]^2)}{E[d_0^{nG}]^2}} \tag{29}$$

The application of this non-Gaussian version of the Low's method requires to know the autocorrelation function $R_Z(\tau)$ of the non-Gaussian process $Z(t)$, the S-N parameters A, k, and in addition the transformation $g(-)$ to be used in Eq. (24) and (27). Other related quantities (e.g. autocorrelation coefficient $\rho_Z(\tau)$, power spectrum $S_Z(f)$, number of half-cycles n, mean upcrossing frequency ν_0^{nG}) are obtained as already explained for the Gaussian case. Note that the transformation $g(-)$ is calibrated based on the skewness and kurtosis, γ_3 and γ_4, that are statistical parameter needed for characterising the non-Gaussian probability law of $Z(t)$. If their exact values are not known, their sample estimates $\hat{\gamma}_3$, $\hat{\gamma}_4$ can be determined from an observed time-history.

5.3 NON-GAUSSIAN SOLUTION BASED ON MADSEN ET AL.´S METHOD

For the Gaussian case, the Madsen et al.'s solution relies on the (approximated) damage autocorrelation coefficient $\rho_{d_0,d_l}^G(l)$ in Eq. (18). As already remarked in Section 4.2, the formula is exact only for $k = 2$, whereas for other values it is approximated, though its level of accuracy seems more than acceptable. On the other hand, this formula has the advantage of being rather simple as it only requires the autocorrelation coefficient of the process, $\rho_X(l)$, and its first time derivative, $\rho_X'(l)$.

Therefore, an attempt is made here to extend the approximated formula in Eq. (18) to the non-Gaussian case, provided that $\rho_Z(l)$ and ν_0^{nG} are used in place of their Gaussian counterparts. From what stated in Section 5.1, and more specifically from the critical analysis of Eq. (21), it is

$\rho_Z(l) \cong \rho_X(l)$. Furthermore, the property that the transformation $G(-)$ has of keeping unaltered the position in time of each value of the Gaussian and non-Gaussian process also ensures that both processes cross their mean values at the same instant of time. Therefore, the Gaussian and non-Gaussian processes have in common the frequency of upward crossings, $\nu_0^{nG} = \nu_0^G$.

For the non-Gaussian process, the autocorrelation coefficient of the damage is then approximated as:

$$\rho_{d_0,d_l}^{nG}(l) \cong \rho_Z^2(l) + \left(\frac{\rho_Z'(l)}{2\pi\nu_0^{nG}}\right)^2 \tag{30}$$

where symbols $\rho_Z(l)$ and ν_0^{nG} have been used only to emphasise that the formula holds for the non-Gaussian case. This formula is given without formal proof, but its level of approximation will be verified by numerical results. Compared to the non-Gaussian Low's method, the coefficient $\rho_{d_0,d_l}^{nG}(l)$ can be obtained with no difficulty, since the transformed JPDF $f_{P_0,P_l}^{nG}(x_p, x_v)$ in Eq. (24) is not involved.

The coefficient $\rho_{d_0,d_l}^{nG}(l)$ in Eq. (30) enters directly into the variance expression in Eq. (13). The other two damage values, $E[d_0^2]$ and $E[d_0]^2$, are determined exactly as for the Low's method for the non-Gaussian case; the fourth property iv) from the list in Section 5.2 remains indeed unchanged. Therefore, the distribution of peaks for non-Gaussian $f_{P_0}^{nG}(z_p)$ follows from a variable transformation of the Rayleigh distribution, see Eq. (26). The terms $E[d_0^{nG}]$ and $E[(d_0^{nG})^2]$ are calculated with Eq. (27).

If all previous results are put together, the approximated expression of the variance of the fatigue damage according to Madsen et al. turns out to be:

$$(\sigma_D^2)_{\mathrm{Mad}}^{nG} = \left\{n + 2\sum_{\mathrm{l}=1}^{\mathrm{n}-1}(\mathrm{n}-\mathrm{l})\left[\rho_{\mathrm{Z}}^2(\mathrm{l}) + \left(\frac{\rho_{\mathrm{Z}}'(\mathrm{l})}{2\pi\nu_0^{\mathrm{nG}}}\right)^2\right]\right\}(E[(d_0^2)^{nG}] - E[d_0^{nG}]^2) \tag{31}$$

The corresponding approximated expression of the CoV is:

$$(C_D)^{nG}_{\mathrm{Mad}} = \frac{1}{n}\sqrt{\left\{n + 2\sum_{l=1}^{n-1}(n-l)\left[\rho_Z^2(l) + \left(\frac{\rho_Z'(l)}{2\pi\nu_0^{nG}}\right)^2\right]\right\}\left(\frac{E[(d_0^2)^{nG}]}{E[d_0^{nG}]^2} - 1\right)} \tag{32}$$

In both equations, the term in curly brackets is identical for both the Gaussian and the non-Gaussian process, as clarified above. The non-Gaussian effect enters, through the transformation $g(-)$, into the last two terms $E[(d_0^2)^{nG}]$ and $E[d_0^{nG}]$.

This non-Gaussian version of the Madsen et al.'s method requires the same quantities previously indicated for the Low's non-Gaussian method, i.e. $R_Z(\tau)$, the S-N parameters and $g(-)$, while other parameters are derived accordingly. In applications, the sample values $\hat{\gamma}_3$, $\hat{\gamma}_4$ estimated from an observed time-history may be used, if the exact values γ_3, γ_4 are not known.

6 NUMERICAL SIMULATIONS

Numerical simulations are used to verify the correctness and accuracy of the two non-Gaussian models described previously. The two models are compared with time-domain results obtained via Monte Carlo method. This numerical study is also used to investigate how the variance and the coefficient of variation vary as a function of the skewness, kurtosis and the S-N inverse slope.

Simulations consider two types of power spectral density for the Gaussian stochastic process $X(t)$: the response of a base-excited linear oscillator and an ideal unimodal (rectangular) power spectrum, see Figure 5.

The linear oscillator is subjected to a band-limited stochastic base acceleration, $W(t)$, with a power spectral density of constant value S_0 and a frequency content from 0 to 20 Hz. Analytical expressions are derived for the mass absolute displacement, $U(t)$, and the relative displacement, $X(t) = U(t) - W(t)$; their mathematical derivation can be found, for example, in Ref. [27]. The final expression of the relative displacement response spectrum is:

$$S_X(f) = \frac{S_0}{(2\pi f_n)^4 \left[\left(1 - \frac{f^2}{f_n^2}\right)^2 + \left(2\zeta \frac{f}{f_n}\right)^2\right]} \tag{33}$$

where f_n is the natural frequency and ζ the damping ratio of the linear oscillator. The system considered in numerical simulations has f_n=10 Hz and a damping ratio taking on three different values $\zeta = 0.005, 0.01, 0.05$. With these values the response spectrum $S_X(f)$ turns out to be a narrow-band stochastic Gaussian process with bandwidth parameters ranging from $\alpha_1 = 0.998$, $\alpha_2 = 0.994$ (for $\zeta = 0.005$) to $\alpha_1 = 0.979$, $\alpha_2 = 0.942$ (for $\zeta = 0.05$). The power spectrum is normalised to unit variance, $\lambda_0 = 1$.

It is important to highlight that, in simulations, the linear oscillator system must be viewed merely as a generator of narrow-band Gaussian time-histories, which are next transformed into non-Gaussian time-histories by $G(-)$. In other words, the oscillator does not represent a nonlinear system that returns a non-Gaussian output when driven by a Gaussian input.

The other power spectral density $S_X(f)$ of $X(t)$ considered in simulations has a unimodal (rectangular) shape centred around frequency f_c (the same as the linear oscillator), and with half-spectral width b that is made to vary from 1 Hz to 10 Hz. By increasing b, the PSD changes from narrow-band to mildly wide-band, with its bandwidth parameters decreasing from $\alpha_1 = 0.998$ and $\alpha_2 = 0.993$ (most narrow-band case) to $\alpha_1 = 0.866$ and $\alpha_2 = 0.745$ (lowest values for the most wide-band case).

A total of $N = 2 \times 10^5$ stochastic Gaussian time-histories $x_i(t)$, $i = 1,2,3, \ldots N$ of time length T are simulated from $S_X(f)$. Three different lengths T are chosen so that time-histories have approximately 10^3, 10^4 and 10^5 fatigue cycles.

Winterstein's model is then used to transform each $x_i(t)$ into a non-Gaussian time-history $z_i(t)$ with prescribed values of skewness γ_3 and kurtosis γ_4. A total of $N = 2 \times 10^5$ time-histories $z_i(t)$ is then obtained. Simulations scrutinise the ranges $0 < \gamma_3^2 < 0.5$ and $2 < \gamma_4 < 8$, which cover

most of the cases of practical interest. It has, however, to be noticed that Winterstein's model imposes some restrictions on the values of γ_3 and γ_4 that can be paired [23].

For each time-history, $x_i(t)$ and $z_i(t)$, the fatigue damage values $D_i^G(T)$ and $D_i^{nG}(T)$ are calculated in time-domain by the rainflow counting and Palmgren-Miner rule. This results into a total of $N = 2 \times 10^5$ damage values for both $D_i^G(T)$ and $D_i^{nG}(T)$, that is, equal to the number of simulated time-histories of $x_i(t)$ and $z_i(t)$. This is the number of realizations used to estimate the variance and coefficient of variation of the damage in time-domain calculations. Damage calculation considers a S-N curve with strength coefficient $A = 1$ and several values of the inverse slope $k = 3, 6, 9$, which cover typical values from notched to smooth components.

The sample mean $\overline{D} = N^{-1} \sum_{i=1}^{N} D_i$, sample variance $\hat{\sigma}_D^2 = (N-1)^{-1} \sum_{i=1}^{N} (D_i - \overline{D})^2$ and sample coefficient of variation $\hat{C}_D = \hat{\sigma}_D / \overline{D}$ are computed from the set of $N = 2 \times 10^5$ damage values available for both the Gaussian and the non-Gaussian case. The expected damage, instead, was computed through analytical solutions: the Gaussian expected damage $E[D^G(T)]$ from Eq. (9), the non-Gaussian expected damage $E[D^{nG}(T)] = 2\nu_0^{nG} T \cdot E[d^{nG}]$ by taking $q = 1$ in Eq. (27).

For the linear oscillator, Figure 6(a) displays the trend of the sample mean $\overline{D}$ and the standard deviation of damage $\hat{\sigma}_D$ (both normalised to the expected damage) for both the Gaussian and the non-Gaussian case, as a function of the number of counted cycles. The figure refers to an inverse slope $k = 3$ and a non-Gaussian process with $\gamma_3 = 0.5$ and $\gamma_4 = 6$.

The box on the left side of Figure 6(a) compares the probability density functions observed, in the non-Gaussian case, for three different numbers of cycles. As the number of cycles (i.e. time-history length) increases, the probability distributions tend to become symmetric and Gaussian, which is in agreement with results observed elsewhere [5]. The comparison of probability distributions demonstrates the increase of the standard deviation as the number of cycles diminishes, which corresponds to a decrease in time-history length. The distributions for the Gaussian case (not shown) are similar in shape, but have a smaller standard deviation – the

comparison of standard deviations is shown in the right side of Figure 6(a). The figure confirms that, in both the Gaussian and non-Gaussian case, the greater is the number of counted cycles, the lower is the dispersion of the damage around its mean value. For any number of cycles, the non-Gaussian damage always has a variance higher than the Gaussian damage. A similar result, not shown here, is observed for other values $\gamma_4 > 3$. This increase in the variance of damage highlights the importance of considering the non-Gaussian effect.

Please insert here Figure 6

The trend in Figure 6(a) is further clarified in Figure 6(b), which shows the change of the CoV versus the number of counted cycles for both methods of Low and Madsen et al. Figure 6(b) refers to an inverse slope $k = 3$ and two different non-Gaussian cases: $\gamma_3 = 0.5$, $\gamma_4 = 2$ (platykurtic) and $\gamma_3 = 0.5$, $\gamma_4 = 6$ (leptokurtic). A perfect matching is observed between time-domain results and theoretical estimations, either Gaussian or non-Gaussian. The agreement in the Gaussian case is somehow predictable [28]. Of more interest here is the correct estimation provided by the non-Gaussian models, whose accuracy is thus verified. Furthermore, the figure also shows that the non-Gaussian models by Low and Madsen et al. are almost equivalent.

The very small, if not almost negligible, discrepancy between theoretical and simulation results in Figure 6(b) has to be attributed to numerical approximations. This approximation tends to occur for kurtosis values $\gamma_4 > 6$ or even greater. One approximation comes from the Winterstein's model, in which there are some best-fitting coefficients. Another approximation source comes from the numerical solution of the double-integral used to compute $E[d_0^{nG} d_l^{nG}]$ through the JPDF $f_{P_0,P_l}^{nG}(z_p, z_v)$ in the Low's model; for very high γ_4 values, the tails of the joint probability distribution tend to be represented not exactly. A final approximation is that adopted in this paper for the Madsen at al.'s approach.

In any case, the largest difference between theory and simulation is 3%, which is perfectly acceptable. In summary, the previous results confirm that the two non-Gaussian models are practically equivalent, and they are not only exact but also cover combinations of skewness and kurtosis over a wide range of values of practical interest, that is within the limits of Winterstein's model $0 < \gamma_3^2 < 2(\gamma_4 - 3)/3$ and $1 < \gamma_4 < 15$.

The simulation results for the ideal unimodal PSD are quite similar to the trends already shown in Figure 6 for the linear oscillator – for this reason, they are not shown in a figure that would be almost identical to Figure 6. Rather, it is of more interest to collect them in a figure displaying the relationship between the CoV of damage and the bandwidth parameter α_1, see Figure 7. Figure 7(b) considers also the results of the linear oscillator (note the different x-axis scale). Both graphs refer to 10^3 counted cycles, two values of inverse slopes ($k = 3, 6$) and a non-Gaussian process with $\gamma_3 = 0.5$, $\gamma_4 = 6$. The solid lines are computed by the theoretical non-Gaussian models (Low, Madsen et al.), whereas the markers are the results from time-domain simulations. In the narrow-band case (α_1 close to unity) the agreement between theory and simulation is very satisfactory. But surprisingly, the agreement remains quite acceptable also in the range of α_1 values characterising a mildly wide-band PSD. The maximum errors is about 19% for the lowest limit value of bandwidth $\alpha_1 = 0.866$ for the unimodal power spectrum. This result is encouraging because it shows that the range of applicability of the non-Gaussian models is not restricted to a strictly narrow-band process, as required by the hypotheses behind the theory. Of course, the accuracy for even wider bandwidths needs to be investigated further.

An overall picture is finally given on the effect of skewness γ_3, kurtosis γ_4 and inverse slope k on the relative variation of the non-Gaussian CoV with respect to the Gaussian case. In particular, Figure 8 shows the trend of the ratio $r = (C_D)^{nG}_{\mathrm{Mad}}/(C_D)^{G}_{\mathrm{Mad}}$ of the coefficient of variation computed by Madsen et al.'s method in either its Gaussian or non-Gaussian version. The Gaussian CoV,

590 $(C_D)^{G}_{\mathrm{Mad}}$, follows from Eq. (20), the non-Gaussian one, $(C_D)^{nG}_{\mathrm{Mad}}$, from Eq. (32). As said above, the estimations $(C_D)^{G}_{\mathrm{Low}}$ and $(C_D)^{nG}_{\mathrm{Low}}$ of the Low's model are almost identical and are thus not shown.

Please insert here Figure 8

Figure 8(a) considers a set of non-Gaussian processes with same skewness $\gamma_3 = 0$, but different values of kurtosis γ_4 and inverse slope k. Compared to the Gaussian case, the CoV of a
595 non-Gaussian process is shown always to decrease ($r < 1$) or increase ($r > 1$) depending on whether the process is platykurtic ($\gamma_4 < 3$) or leptokurtic ($\gamma_4 > 3$). For a given γ_4, the variation depends on k.

In the region $\gamma_4 < 3$, the decrease of CoV becomes larger for high k values. For $\gamma_4 = 2$, the CoV diminishes up to 60% for $k = 9$. In the region $\gamma_4 > 3$ the CoV has an opposite trend, but k has
600 a more pronounced effect, especially when $k > 3$. For example, for $k = 6$ the increase arrives at 120% for $\gamma_4 = 6.3$, whereas for $k = 9$ the same increase is attained already for γ_4 slightly below 4.

Figure 8(b) shows, instead, the effect of skewness γ_3 on the CoV of damage of "asymmetric" stochastic processes. The kurtosis is set to $\gamma_4 = 3.5$; it is indeed not possible to choose a lower value if, in the Winterstein's model, the skewness has to reach the limits -0.5 to
605 +0.5. Similar trends are obtained for other γ_4 values.

For any given k, the curves in Figure 8(b) are symmetric, which is yet not surprising. In fact, in the Winterstein's model, the transformation $G(-)$ corresponding to equal and opposite values $+\gamma_3$ and $-\gamma_3$ turns out to be "mirrored" with respect to the straight line of the Gaussian case. In symbols: $G_{\gamma_3>0}(X) = -G_{\gamma_3<0}(-X)$. Skewness values other than zero only make the mean stress of
610 each non-Gaussian cycle, $(z_p + z_v)/2$, be different from zero, whereas stress amplitudes remain unchanged and follow the same probability distribution in both cases $+\gamma_3$ and $-\gamma_3$.

The results in Figure 8(b) reveals that for a given γ_4, the largest increment of CoV occurs for $\gamma_3 = 0$; lower increments are observed for either positive or negative skewness values. As

before, the higher the inverse slope k, the higher the increment, although now the effect is less marked than what observed for the kurtosis. In any case, these results confirm once more the importance of considering non-Gaussian effects in the evaluation of the variance of damage.

7 COMPUTATION OF THE FAILURE PROBABILITY: A CASE STUDY

The previous Sections emphasised that the fatigue damage $D(T)$ of a stochastic time-history $x(t)$ of length T is a random variable following a certain probability density function. This probability distribution changes depending on whether the time-history is Gaussian or non-Gaussian. An example for the non-Gaussian case is shown in Figure 6(a). With the aim to apply the Gaussian and non-Gaussian models (Madsen et al.'s method) for the variance of damage, this section presents a case study of a real-world application. In this case study, the failure probabilities of Gaussian and non-Gaussian time-histories are compared after computing the expected damage and variance of the damage probability distributions directly from the "exact" stress power spectrum, which is known through an equation and thus has no statistical variability.

According to the Palmgren-Miner rule, the fatigue failure occurs when the damage $D(T)$ reaches a critical value D_{cr}. A failure probability P_f is thus associated with the event $D(T) > D_{cr}$. This failure probability will depend on the Gaussian or non-Gaussian nature of the stochastic time-history, as well as on the statistical scatter of D_{cr}. In fact, though the Palmgren-Miner rule postulates that D_{cr} is a deterministic value equal to one, extensive experimental studies confirmed that D_{cr} is scattered and follows a lognormal distribution, see Figure 9 (this figure, originally published in Ref. [29], is reported also in many other articles, e.g. [30]). Similar trends for other alloys are published elsewhere [31].

The probability distributions involved in the computation of the failure probability are exemplified in Figure 10. Figure 10(a) shows the definition of the characteristic S-N line corresponding to a prescribed failure probability under constant amplitude loading. The S-N line

parameters k, A then include the scatter observed in constant amplitude tests. Figure 10(b) shows, instead, the damage distributions.

The approach here described takes two sources of statistical variability into account simultaneously: the uncertainty/scatter of the damage $D(T)$ due to the finite duration of the stochastic time-history, and the dispersion of the critical damage D_{cr} of the Palmgren-Miner rule as it is observed from experiments. The probability of failure turns out to be [4]:

$$P_f = Prob\{D(T) > D_{cr}\} = \int_{-\infty}^{\infty} f_D(x) \cdot F_{D_{cr}}(x) dx \tag{34}$$

where $f_D(x)$ is the probability density function of the fatigue damage $D(T)$ and $F_{D_{cr}}(x)$ the cumulative distribution function of the critical damage D_{cr}. The probability distribution $f_D(x)$ can be estimated from observed damage values, as the example in Figure 4, or assumed to be normally distributed as suggested in [20]. The cumulative distribution $F_{D_{cr}}(x)$ can be fitted on observed values of the critical damage, see for example Figure 9, which refers to the normal probability plot of $log(D_{cr})$. The probability on the vertical axis represents the complementary cumulative distribution function $1 - F_{D_{cr}}\big(log(D_{cr})\big)$. The plot confirms the scattered nature of D_{cr}, showing that 90% of the data fall below the conventional value $D_{cr} = 1$ while only 10% are above. The median and standard deviation of $log(D_{cr})$ listed in Table 1 are derived from Figure 9 by the procedure of Appendix B.

The importance of including non-Gaussian time-history characteristics in the computation of the failure probability P_f is now demonstrated by an example. It will show how a non-Gaussian random time-history determines an increased failure probability P_f compared to the case of a Gaussian time-history with same variance.

The example considers the output stochastic stress in an offshore platform subjected to a non-stationary wave loading, formed by eleven sea states (Figure 11). The significant wave height

660 H_s and dominant wave period T_D of each sea state (see Table 2) define the stress power spectral density [32,33]:

$$S(f) = \frac{G H_s^{\varphi} \exp\left[-\frac{1050}{(2\pi f T_D)^4}\right]}{T_D^4 (2\pi f)^5 \left[\left(1 - \frac{f^2}{f_n^2}\right)^2 + \left(\frac{2\zeta f}{f_n}\right)^2\right]} \tag{35}$$

Symbols $G = 5580$ and $\varphi = 3.25$ are scaling factors, whereas $\zeta = 0.02$ (damping ratio) and $f_n = 0.286$ Hz (first resonance frequency) characterize the offshore dynamic response. The previous PSD expression combines the Pierson-Moskowitz wave spectrum with the frequency response
665 function of the offshore platform simplified as a simple oscillator.

The output stress, with power spectrum $S(f)$, is assumed to be either Gaussian, $x(t)$, or non-Gaussian, $z(t)$. This is used to quantify and compare the non-Gaussian effects on the calculated failure probability P_f. While the Gaussian time-history has zero skewness and kurtosis three, the non-Gaussian time-history is assumed to have two combinations of skewness and
670 kurtosis, namely skewness zero and kurtosis from 3 to 6, or skewness from -0.4 to 0.4 with kurtosis 3.5 – this allows for a sensitivity analysis.

The random stress $x(t)$ and $z(t)$ have an identical standard deviation, with values for each sea state are specified in Table 2. Also an identical total time duration T is taken for both $x(t)$ and $z(t)$. The values $T = 5, 7, 9$ years are considered for comparison purposes. The total length $T = \sum_i T_i$ sums the length of individual sea states. Once a value of T is chosen, the individual lengths T_i are determined according to the time fractions listed in Table 2. Note that the individual length T_i merely represents the portion of the total time T spent by the offshore platform in *i*-th sea state, independently of the sea state sequence. In fact, the offshore platform needs not to stay in the *i*-th state for the whole time T_i, nor to pass through all the different sea states consecutively. The
680 sequence of sea states can be random, as it actually happens in reality. Summing up the time sub-fractions spent in each sea state corresponds to ignoring the cycles formed by peaks and valleys

falling in different sea states, which holds true if the length of each sea state is not close to zero. This also makes the damage values from different sea state independent [20].

The total damage $D(T)$ for the length T is the sum of the damage $D_i(T_i)$ contributed by each individual sea state of length T_i, that is $D(T) = \sum_i D_i(T_i)$. Each individual damage $D_i(T_i)$ is assumed to follow a normal distribution; this hypothesis is acceptable in so far as T_i is long enough for the central limit theory to apply [5]. As the total damage $D(T)$ is the sum of independent and normally distributed damage values $D_i(T_i)$, its statistics are simply $E[D(T)] = \sum_i E[D_i(T_i)]$ and $\sigma_D^2 = \sum_i \sigma_{D_i}^2$.

The parameters (expected value, variance) of the normal distribution of $D_i(T_i)$ are determined as follows. For the Gaussian case, the expected damage $E\left[D_i^G(T)\right]$ follows from Eq. (9), while the variance $\left(\sigma_{D_i}^2\right)^G$ from Eq. (19) (Madsen et al.'s method). For the non-Gaussian case, the expected damage $E\left[D_i^{nG}(T)\right]$ follows from Eq. (27) with $q = 1$, while the variance $\left(\sigma_{D_i}^2\right)^{nG}$ from Eq. (31) (Madsen et al.'s method).

The analysis finally assumes that $x(t)$ and $z(t)$ represent the stress acting on a welded structural detail. The characteristic S-N curve of this detail has inverse slope $k = 4$ and fatigue strength coefficient $A = 7.688 \times 10^{13}$ MPa [32,33]. Accordingly, the probability distribution of D_{cr} takes the parameters for welded steel members.

The obtained results are summarised in Figure 12, which displays the ratio P_f^{nG}/P_f^G of the failure probabilities corresponding, respectively, to a Gaussian and non-Gaussian time-history, all other analysis parameters being kept unchanged. The ratio is plotted for different values of skewness and kurtosis, and time-history length. The increase in the failure probability due to non-Gaussian effects stands out clearly. For a given time-history length, the increase of the ratio P_f^{nG}/P_f^G is much more sensitive to the kurtosis than to the skewness.

For a given time-history length T, the variation of the ratio P_f^{nG}/P_f^G is much more affected by a change in kurtosis than in skewness.

For a given time-history length T, the ratio P_f^{nG}/P_f^G varies more markedly with a change in kurtosis than in skewness.

For example, for a time-history length of $T = 5$ years, the ratio changes of about some hundreds when the kurtosis varies from three to 5, whereas it only changes of several units when skewness varies from zero to ± 0.2. Note also that the ratio follows opposite trends, since it increases with kurtosis but decreases with skewness. For a given non-Gaussian behaviour (that is, for given values of skewness and kurtosis), the ratio of failure probabilities P_f^{nG}/P_f^G grows as the time-history length T decreases. This trend is governed by the shape of the upper tail of the damage distribution that, in turn, "intersects" the distribution of the critical damage D_{cr} as in Eq. (34). When the time T decreases, both Gaussian and non-Gaussian damage distributions shift to the left, since their expected value and variance are proportional to T – see the theoretical results in Section 3. By contrast, the probability distribution of critical damage D_{cr} remains fixed. As a result of this shift in damage distributions, the amount of area "beyond" D_{cr} (and which actually determines the failure probability as per Eq. (34)) changes in different ways, so that the ratio P_f^{nG}/P_f^G becomes greater for a shorter time duration.

Apart from the different trends commented above, Figure 12 highlights that the failure probability is underestimated if non-Gaussian effects are ignored by the reliability analysis. This, in turns, confirms the importance of including non-Gaussian effect when assessing the structural durability.

8 CONCLUSIONS

The paper presented two theoretical models for assessing the variance of the fatigue damage in stationary non-Gaussian stochastic processes. The non-Gaussian models extend two methods existing in the literature (Madsen et al., Low's) that are valid for Gaussian narrow-band processes. The two models here developed apply to any non-Gaussian process for which its narrow-band power spectral density, skewness and kurtosis coefficients are known. They exploit the properties of a time-independent non-linear transformation that establishes a relationship between Gaussian and non-Gaussian domains.

Monte Carlo numerical simulations in time-domain approach were used to verify the correctness and accuracy of the proposed two models and to identify typical trends. A linear oscillator response and a unimodal PSD were considered to simulate a large sample of both Gaussian and non-Gaussian time-histories, of which the fatigue damage was computed in time-domain. The statistics (mean value, standard deviation, coefficient of variation) characterising the sample of computed damage values were compared to theoretical estimations. A perfect matching was observed. The results also demonstrated that, in the non-Gaussian case, the fatigue damage has a higher variance compared to the Gaussian case. This result is of particular importance as it confirms that the inappropriate use of Gaussian models with non-Gaussian processes leads to unsafe predictions, as they neglect non-Gaussian effects. The use of the non-Gaussian models here proposed is then recommended.

The paper then investigated the trends of the coefficient of variation (CoV) of damage as a function of three parameters: skewness γ_3, kurtosis γ_4, and inverse slope k of S-N curve.

Non-Gaussian effects make the CoV increase or decrease with respect to its value in the Gaussian case; which type of trend and its extent is mostly influenced by the kurtosis value and, to a less degree, by the skewness value. Compared to the Gaussian case ($\gamma_3 = 0$, $\gamma_4 = 3$), the coefficient of variation decreased for $\gamma_4 < 3$ and increased for $\gamma_4 > 3$, the amount of the variation being

further modulated by the inverse slope k. In particular, the worst combination that gives the highest increase of CoV occurs when both kurtosis and inverse slope take on large values. For example, the coefficient of variation increases far beyond 350% if kurtosis $\gamma_4 > 4$ and the inverse slope $k > 6$ (a value typical of un-notched structural details). These results, too, highlight even more the need of including the non-Gaussian effects when estimating the variance of the damage in a non-Gaussian stochastic process.

An example of an offshore platform under different sea states is finally discussed. The example is used to demonstrate the increase of the failure probability due to the non-Gaussian characteristics of the stochastic time-history. The increase markedly depends on the kurtosis value and can be as large as nine for a kurtosis around six, when the time-history length is five years. The example then further emphasises the importance of taking non-Gaussian effects into account in a structural durability analysis with stochastic loadings.

APPENDIX A

This Section reviews the Winterstein's model based on Hermite polynomials. In particular, the Section reports the expressions of both the direct and the inverse transformation, $G(-)$ and $g(-)$, though only the latter function along with its first derivative are used by the models developed in Section 5.

The expressions of the transformation model are provided separately for two types of non-Gaussian process: leptokurtic ($\gamma_4 > 3$) and platykurtic ($\gamma_4 < 3$).

For a leptokurtic process ($\gamma_4 > 3$), the direct transformation links the non-Gaussian process $Z = G(X_0)$ to a standardised Gaussian process $X_0 = (X - \mu_X)/\sigma_X$, where process X has mean value μ_X and standard deviation σ_X (the time t variable is omitted for clarity). The direct transformation is defined as [23]:

$$G(X_0) = \mu_Z + \kappa\sigma_Z[X_0 + c_3(X_0^2 - 1) + c_4(X_0^3 - 3X_0)] \tag{36}$$

where μ_Z is the mean value and σ_Z the standard deviation of the non-Gaussian process; the coefficients c_3, c_4 and κ are detailed below. Inversion of the previous expression yields the inverse transformation as [23]:

$$g(Z) = \left[\sqrt{\xi^2(Z) + c} + \xi(Z)\right]^{\frac{1}{3}} - \left[\sqrt{\xi^2(Z) + c} - \xi(Z)\right]^{\frac{1}{3}} - a \tag{37}$$

where:

$$\xi(Z) = 1.5b\left(a + \frac{Z - \mu_Z}{\kappa\sigma_Z}\right) - a^3 \tag{38}$$

in which $a = c_3/(3c_4)$, $b = 1/(3c_4)$, $c = (b - 1 - a^2)^3$. In both the direct and inverse transformation, κ is a scale factor assuring that both the Gaussian and non-Gaussian process have a common value of variance, $\sigma_X^2 = \sigma_Z^2$.

The coefficients c_3, c_4 and κ take on slightly different expressions depending on the various versions of the method. The earliest version [9] was a first-order model limited to small non-Gaussian degrees; it returned the coefficient expressions:

$$c_3 = \frac{\gamma_3}{6}; \qquad c_4 = \frac{(\gamma_4 - 3)}{24}; \quad \kappa = 1 \tag{39}$$

A more accurate approximation including also second-order terms into the Hermite model (second-order model) gave the following coefficients [22]:

$$c_3 = \frac{\gamma_3}{6(1 + 6c_4)}; \qquad c_4 = \frac{\sqrt{1 + 1.5(\gamma_4 - 3)} - 1}{18}; \quad \kappa = \frac{1}{\sqrt{1 + 2c_3^2 + 6c_4^2}} \tag{40}$$

An alternative version also exists, with the following coefficient expressions [23]:

$$c_3 = \frac{\gamma_3}{6}\left[\frac{1 - 0.015|\gamma_3| + 0.3\gamma_3^2}{1 + 0.2(\gamma_4 - 3)}\right]; \qquad c_4 = c_{40}\left(1 - \frac{1.43\gamma_3^2}{\gamma_4 - 3}\right)^{1 - 0.1\gamma_4^{0.8}} \tag{41}$$

where

$$c_{40} = \frac{[1 + 1.25(\gamma_4 - 3)]^{1/3} - 1}{10} \tag{42}$$

These coefficients hold for $0 < \gamma_3^2 < 2(\gamma_4 - 3)/3$ and $3 < \gamma_4 < 15$, which include most non-Gaussian cases.

For a platykurtic process ($\gamma_4 < 3$), the inverse transformation is:

$$g(Z) = Z_0 - c_3(Z_0^2 - 1) - c_4(Z_0^3 - 3Z_0) \tag{43}$$

where $Z_0 = (Z - \mu_Z)/\sigma_Z$ is a standardised process and c_3, c_4 are coefficients already defined above.

It has finally to be reminded that not all combinations of γ_3, γ_4 values are actually allowed by the Winterstein's model. For more details, see [22].

APPENDIX B

The mean μ and standard deviation σ of the lognormal distribution of D_{cr} can be determined from two percentiles of the normal probability plot in Figure 9, after such a plot is fitted to a sample of experimental data. Let $D_{cr,i}$, P_i $(i = 1,2)$ be two pairs of values (damage, probability) read from Figure 9. A choice could be $P_1 = 10\%$ and $P_2 = 90\%$. The log-transformed variable is $x_i = log(D_{cr,i})$, while the cumulative probability is $p_i = (1 - P_i)$.

As $Z = (log(D_{cr}) - \mu)/\sigma$ is a standard normal variable, the probability statement $Pr[log(D_{cr}) \leq x_i] = p_i$ is equivalent to:

$$Pr\left(Z \leq \frac{x_i - \mu}{\sigma}\right) = \Phi\left(\frac{x_i - \mu}{\sigma}\right) = p_i \tag{44}$$

which yields two linear equations:

$$\Phi^{-1}(p_i)\sigma + \mu = x_i \quad (i = 1, 2) \tag{45}$$

with the solution:

$$\sigma = \frac{x_2 - x_1}{\Phi^{-1}(p_2) - \Phi^{-1}(p_1)} \qquad \mu = \frac{x_1\Phi^{-1}(p_2) - x_2\Phi^{-1}(p_1)}{\Phi^{-1}(p_2) - \Phi^{-1}(p_1)} \tag{46}$$

Table 1 lists the statistical parameters obtained by the above procedure applied to the four normal probability plots of Figure 9. Small approximations, due to the reading of values directly from the figure, may be present.

REFERENCES

1 Benasciutti D, Tovo R. Frequency-based Analysis of Random Fatigue Loads: Models, hypotheses, reality. Materialwiss Werkstofftech 2018;49(3):345-367. https://doi.org/10.1002/mawe.201700190.

2 Mark WD. The Inherent Variation in Fatigue Damage Resulting from Random Vibration. Ph.D. Thesis, Department of Mechanical Engineering, M.I.T.; 1961.

3 Bendat JS. Probability Functions for Random Responses: Prediction of Peaks, Fatigue Damage, and Catastrophic Failures. NASA CR-33; 1964.

4 Madsen HO, Krenk S, Lind NC. Methods of structural safety. Englewood Cliffs: Prentice-Hall; 1986.

5 Low YM. Variance of the fatigue damage due to a Gaussian narrowband process. Struct Saf 2012;34(1):381–9. https://doi.org/10.1016/j.strusafe.2011.09.001

6 Bengtsson A, Bogsjö K, Rychlik I. Uncertainty of estimated rainflow damage for random loads. Mar Struct 2009;22:261–274. https://doi:10.1016/j.marstruc.2008.05.001

7 Bendat JS, Piersol AG. Random data: analysis and measurement procedures. New York: Wiley-Interscience; 1986.

8 Lutes LD, Sarkani S. Random vibrations: analysis of structural and mechanical systems. Elsevier; 2004.

9 Winterstein SR. Non-normal responses and fatigue damage. J Eng Mech ASCE 1985;111(10):1291-95. https://doi.org/10.1061/(ASCE)0733-9399(1985)111:10(1291)

10 Winterstein S. Moment-based Hermite models of random vibration. Report No. 2019, Dept. of Structural Engineering, technical University of Denmark, Lyngby, Denmark, 1987.

11 Grigoriu M. Simulation of stationary non-Gaussian translation processes. J Eng Mech 1998;124(2): 121-126. https://doi.org/10.1061/(ASCE)0733-9399(1998)124:2(121)

12 Grigoriu M. Existence and construction of translation models for stationary non-Gaussian processes. Prob Eng Mech 2009;24(4):545-551. https://doi.org/10.1016/j.probengmech.2009.03.006

13 Grigoriu M. Non-Gaussian models for stochastic mechanics. Prob Eng Mech 2000;15(1):15-23. https://doi.org/10.1016/S0266-8920(99)00005-3

14 FKM Guideline. Analytical strength assessment of components in mechanical engineering. 5th ed., Frankfurt: FKM, 2003.

15 Miles JW. On structural fatigue under random loading. J Aeron Sci 1954;21(11):753–62. https://doi.org/10.2514/8.3199

16 Rice SO. Mathematical analysis of random noise. Bell Syst Tech J 1945;23:282–32. https://doi.org/10.1002/j.1538-7305.1945.tb00453.x

17 Benasciutti D. The role of uncertainty of power spectral density data in estimating the fatigue damage of random uniaxial loadings through frequency-domain methods. In: Proceedings of the Fourth International Conference on Material and Component Performance under Variable Amplitude Loading (VAL4), 30 March to 1 April 2020, Darmstadt, Germany, DVM, Berlin, pp. 91–100.

18 Krenk S, Madsen PH. Stochastic response analysis. In: Thoft-Christensen P, editor. Reliability theory and its application in structural and soil mechanics. NATO Advanced Study Institute Series, Springer-Verlag; 1983, p. 103–172.

19 Langley RS. On various definitions of the envelope of a random process. J Sound Vib 1986; 105(3):503-512. https://doi.org/10.1016/0022-460X(86)90175-6

20 Marques JME, Benasciutti D, Tovo R. Variability of the fatigue damage due to the randomness of a stationary vibration load. Int J Fatigue 2020;141:105891. https://doi.org/10.1016/j.ijfatigue.2020.105891

21 Ochi MK, Ahn K. Probability distribution applicable to non-Gaussian random processes. Prob Eng Mech 1994;9:255–64. https://doi.org/10.1016/0266-8920(94)90017-5

22 Winterstein SR. Nonlinear vibration models for extremes and fatigue. J Eng Mech ASCE 1988;114(10):1772–90. https://doi.org/10.1061/(ASCE)0733-9399(1988)114:10(1772)

23 Winterstein SR, Ude TC, Kleiven G. Springing and slow-drift responses: predicted extremes and fatigue vs. simulation. In: BOSS'94 Proceedings of the seventh international conference on the behaviour of offshore structures, M.I.T.; 1994.

24 Kihl DP, Sarkani S, Beach JE. Stochastic fatigue damage accumulation under broadband loadings. Int J Fatigue 1995;17(5):321–9. https://doi.org/10.1016/0142-1123(95)00015-L

25 Sarkani S, Kihl DP, Beach JE. Fatigue of welded joints under narrowband non-Gaussian loadings. Prob Eng Mech 1994;9:179–90. https://doi.org/10.1016/0266-8920(94)90003-5

26 Smallwood DO. Generating non-Gaussian vibration for testing purposes. Sound and Vibration 2005;39(10):18–24.

27 Wirsching PH, Paez TL, Ortiz K. Random vibrations: Theory and practice. New York: John Wiley & Sons; 1995.

28 Marques JME, Benasciutti D, Tovo R. Variance of fatigue damage in stationary random loadings: comparison between time- and frequency-domain results. Proc Struct Integrity 2019;24:398-07. https://doi.org/10.1016/j.prostr.2020.02.037

29 Eulitz K-G, Kotte KL. Damage accumulation-limitations and perspectives for fatigue life assessment. Proc Mater Week, Frankfurt 2000.

30 Sonsino CM Fatigue testing under variable amplitude loading. Int J Fatigue 2007;29:1080-1089. https://doi.org/10.1016/j.ijfatigue.2006.10.011

31 Beretta S, Regazzi D. Probabilistic fatigue assessment for railway axles and derivation of a simple format for damage calculations. Int J Fatigue 2016; 86: 13-23. https://doi.org/10.1016/j.ijfatigue.2015.08.010

32 Wirsching PH. Fatigue reliability in welded joints of offshore structures. Int J Fatigue 1980;2(2):77-83. https://doi.org/10.1016/0142-1123(80)90035-3

33 Chaudhury GK, Dover WD. Fatigue analysis of offshore platforms subject to sea wave loadings. Int J Fatigue 1985;7(1):13-19. https://doi.org/10.1016/0142-1123(85)90003-9

TABLES

Table 1. Median and standard deviation of the critical damage sum D_{cr}, as estimated from Figure 9.

Structural detail	Alloy type	Median, $10^{\mu_{\log(D_{cr})}}$	Standard deviation, $\sigma_{\log(D_{cr})}$
Not welded	Steel	0.28	0.40
	Aluminium	0.38	0.39
Welded	Steel	0.44	0.24
	Aluminium	0.27	0.46

900

Table 2. Sea state data.

Sea state	Fraction of time T_i/T	Significant wave height, H_s	Dominant wave period, T_D	Standard deviation of the stress
A	0.19	0.76	4.4	1.7
B	0.49	2.28	7.7	4.32
C	0.21	3.81	9.1	7.87
D	0.06	5.33	10.3	11.67
E	0.03	6.86	11.6	15.54
F	0.01	8.38	12.7	19.89
G	0.007	9.9	13.6	24.78
H	0.002	11.43	14.7	29.81
I	0.0004	12.96	15.8	35.19
J	0.0001	14.48	16.5	41.32
K	0.00004	16.01	17.3	47.72

905

FIGURE CAPTIONS

Figure 1. Approximated damage autocorrelation coefficient $\rho^{G}_{d_0,d_l}(l)$ in Eq. (18), compared with simulations. Unimodal PSD.

Figure 2. (a) Relationship between the values $X(t)$ and $Z(t) = G(X(t))$ for a linear and non-linear transformation $G(-)$; (b) Gaussian and its corresponding transformed non-Gaussian stochastic process (dashed line refers to Gaussian and solid line to non-Gaussian).

Figure 3. Comparison between the Gaussian and non-Gaussian autocorrelation coefficient, for two combinations of skewness γ_3, kurtosis γ_4, and spectral bandwidth b (ideal PSD).

Figure 4. (a) Joint probability density function of peaks and (b) its marginal probability density function of peaks.

Figure 5. Power spectral densities used in numerical simulations: (a) linear oscillator system (for two limit values of damping), (b) ideal unimodal spectrum (the dashed and the continuous line show the PSD with the narrowest and the widest half-spectral bandwidth).

Figure 6. Simulation results for the linear oscillator as a function of the number of counted cycles (damping $\zeta = 0.005$, inverse slope $k = 3$): (a) sample mean and sample standard deviation of the damage (both normalised to the expected damage); the left panel shows the observed probability distributions (non-Gaussian case). (b) coefficient of variation of damage.

Figure 7. Trends of the CoV as a function of the bandwidth parameter α_1, for (a) linear oscillator and (b) ideal unimodal PSD. Solid lines are the theoretical estimations, markers come from time-domain simulations.

Figure 8. Ratio of coefficient of variation of damage $r = (C_D)^{nG}_{\mathrm{Mad}}/(C_D)^{G}_{\mathrm{Mad}}$ versus (a) kurtosis coefficient and (b) skewness coefficient, for several values of the inverse slope k of the S-N curve.

Figure 9. Statistical distribution of the real damage sum (critical damage) for steel and aluminium. (Reprinted from Sonsino CM Int J Fatigue 2007;29:1080-1089, with permission from Elsevier)

Figure 10. (a) Characteristic S-N line including the variability of fatigue strength; (b) probability distributions involved in the computation of the failure probability.

Figure 11. Offshore platform under wave loading, with a Gaussian or non-Gaussian time-history
935 acting on a critical welded joint

Figure 12. Increment of the failure probability due to a non-Gaussian time-history with: (a) skewness $\gamma_3 = 0$ and kurtosis γ_4 from 3 to 6; (b) kurtosis $\gamma_4 = 3.5$ and skewness from -0.4 to 0.4.

FIGURES

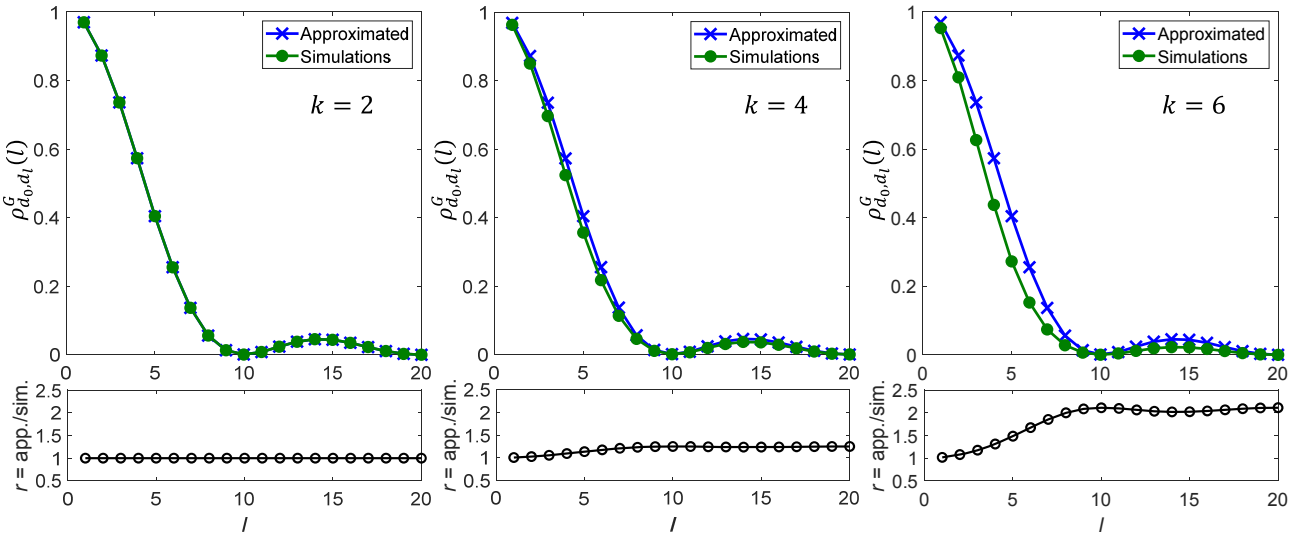

Figure 1. Approximated damage autocorrelation coefficient $\rho^G_{d_0,d_l}(l)$ in Eq. (18), compared with simulations. Unimodal PSD.

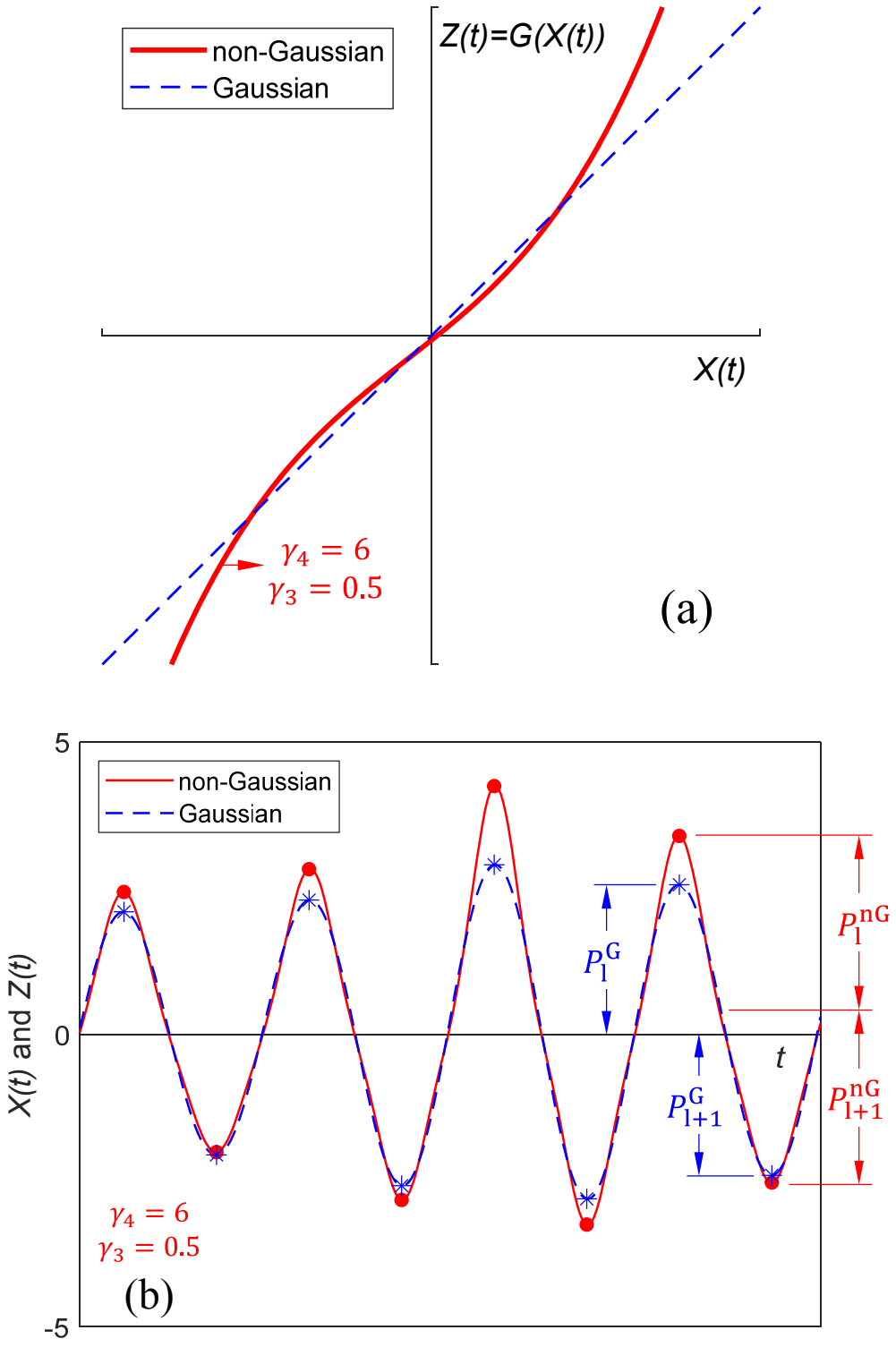

Figure 2. (a) Relationship between the values $X(t)$ and $Z(t) = G(X(t))$ for a linear and non-linear transformation $G(-)$; (b) Gaussian and its corresponding transformed non-Gaussian stochastic process (dashed line refers to Gaussian and solid line to non-Gaussian).

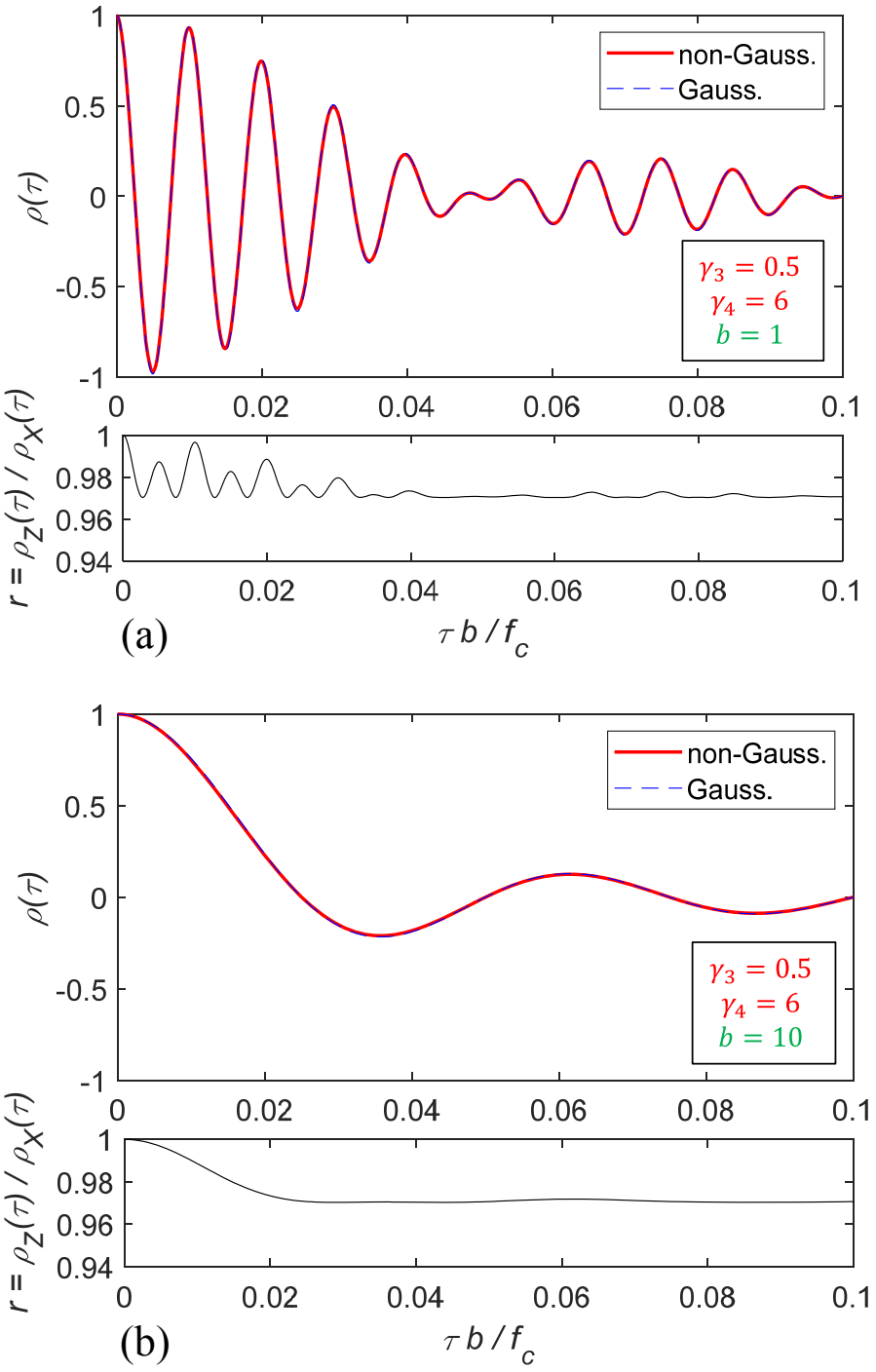

Figure 3. Comparison between the Gaussian and non-Gaussian autocorrelation coefficient, for two combinations of skewness γ_3, kurtosis γ_4, and spectral bandwidth b (ideal PSD).

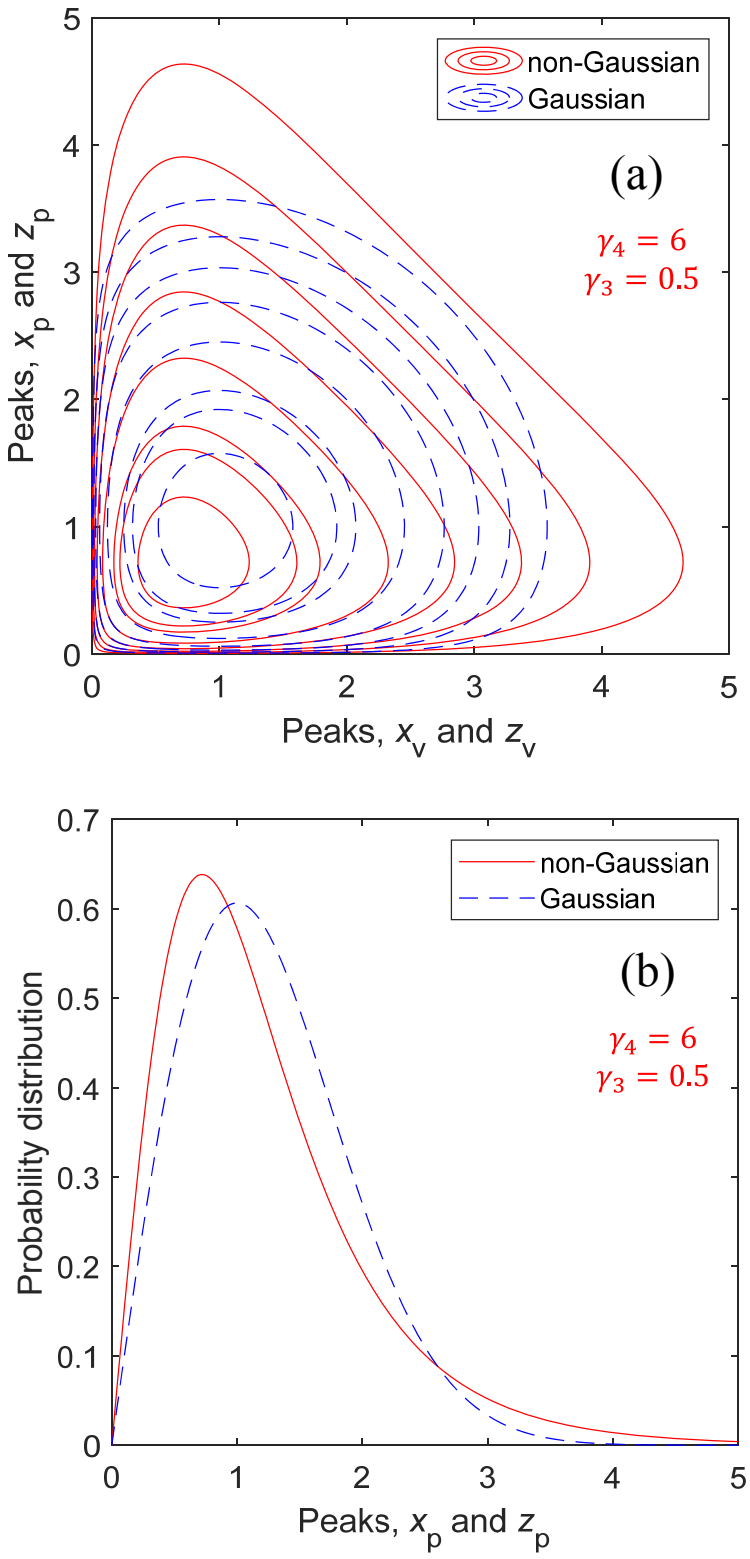

Figure 4. (a) Joint probability density function of peaks and (b) its marginal probability density function of peaks.

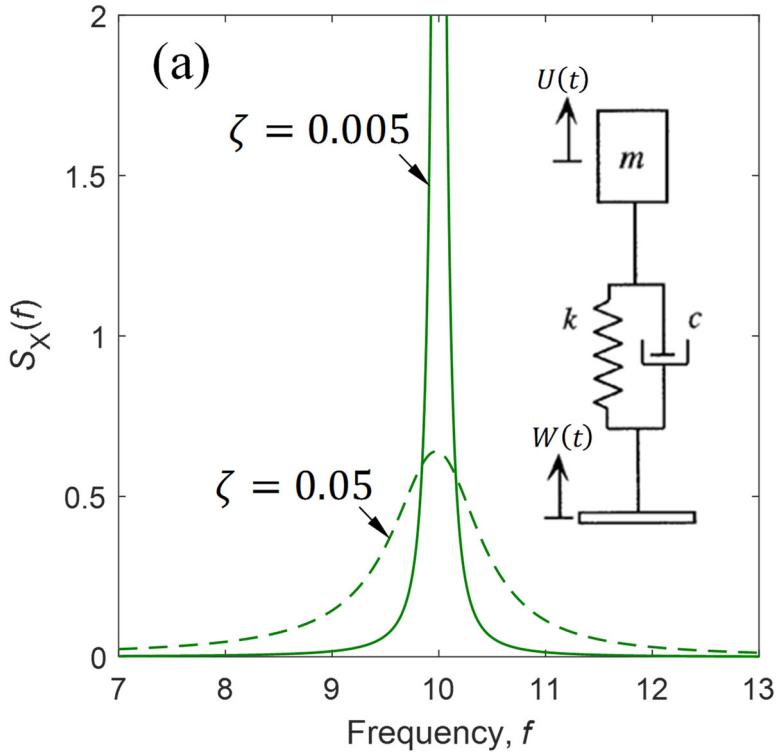

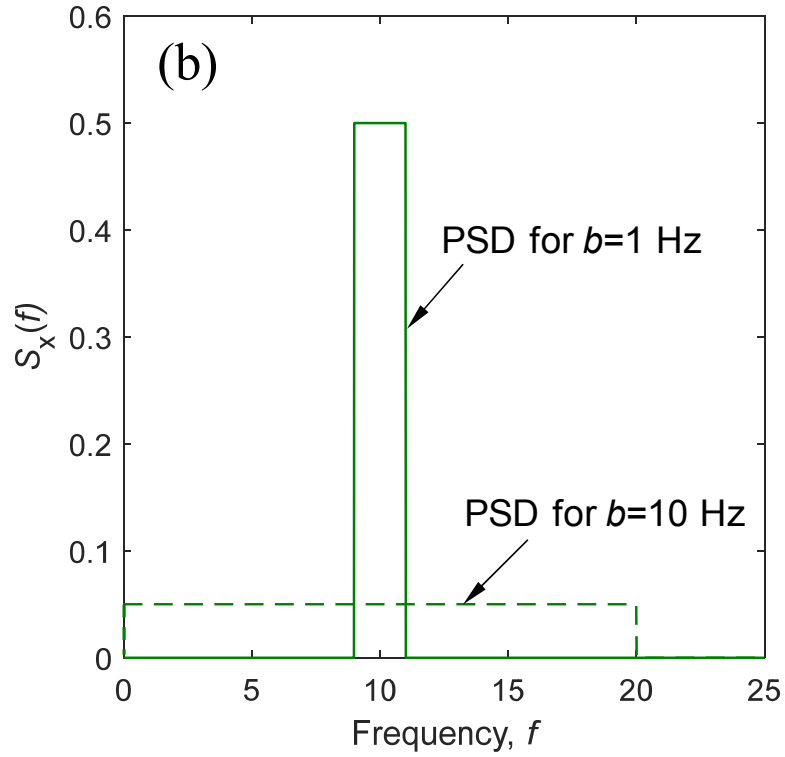

Figure 5. Power spectral densities used in numerical simulations: (a) linear oscillator system (for two limit values of damping), (b) ideal unimodal spectrum (the dashed and the continuous line show the PSD with the narrowest and the widest half-spectral bandwidth).

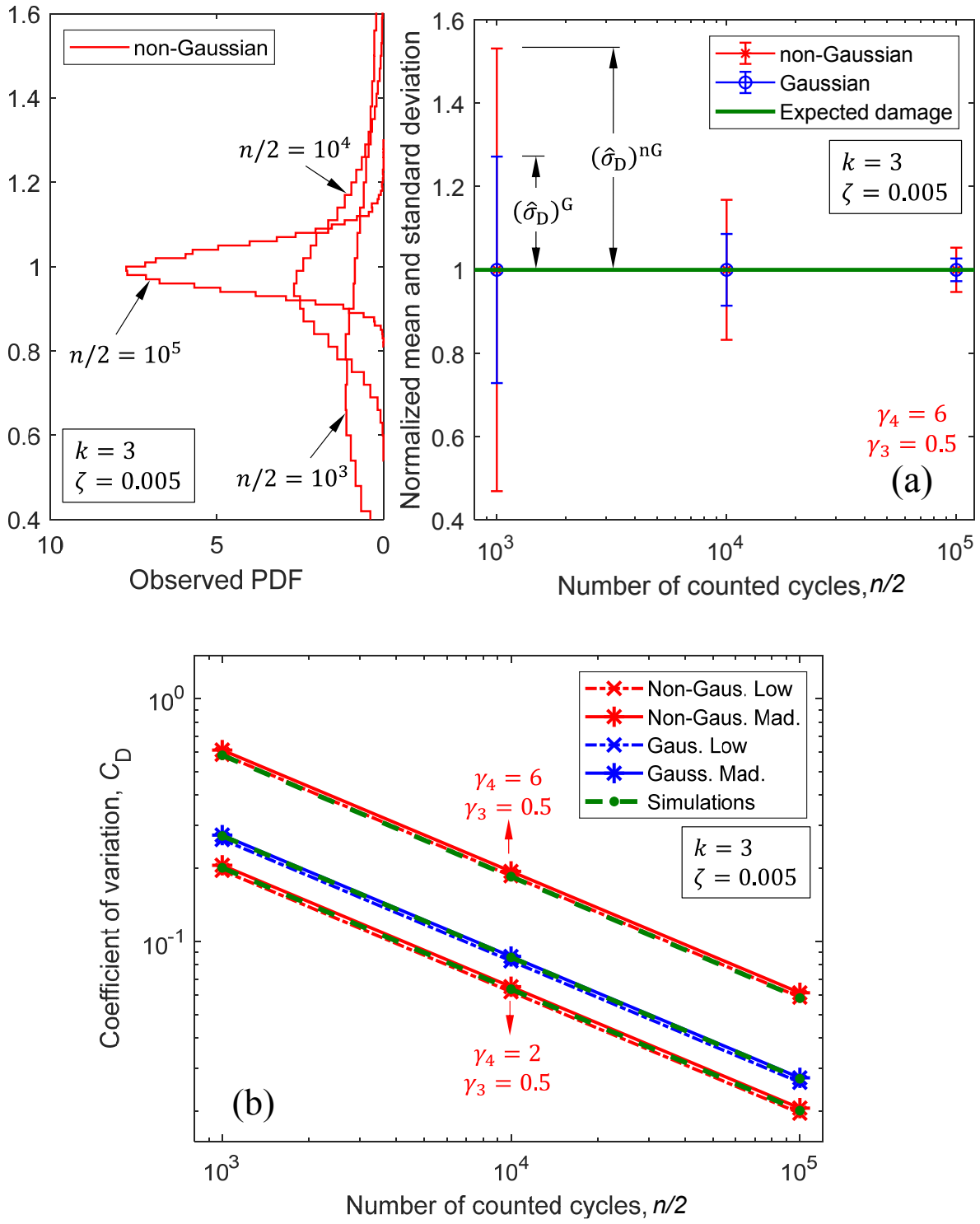

Figure 6. Simulation results for the linear oscillator as a function of the number of counted cycles (damping $\zeta = 0.005$, inverse slope $k = 3$): (a) sample mean and sample standard deviation of the damage (both normalised to the expected damage); the left panel shows the observed probability distributions (non-Gaussian case). (b) coefficient of variation of damage.

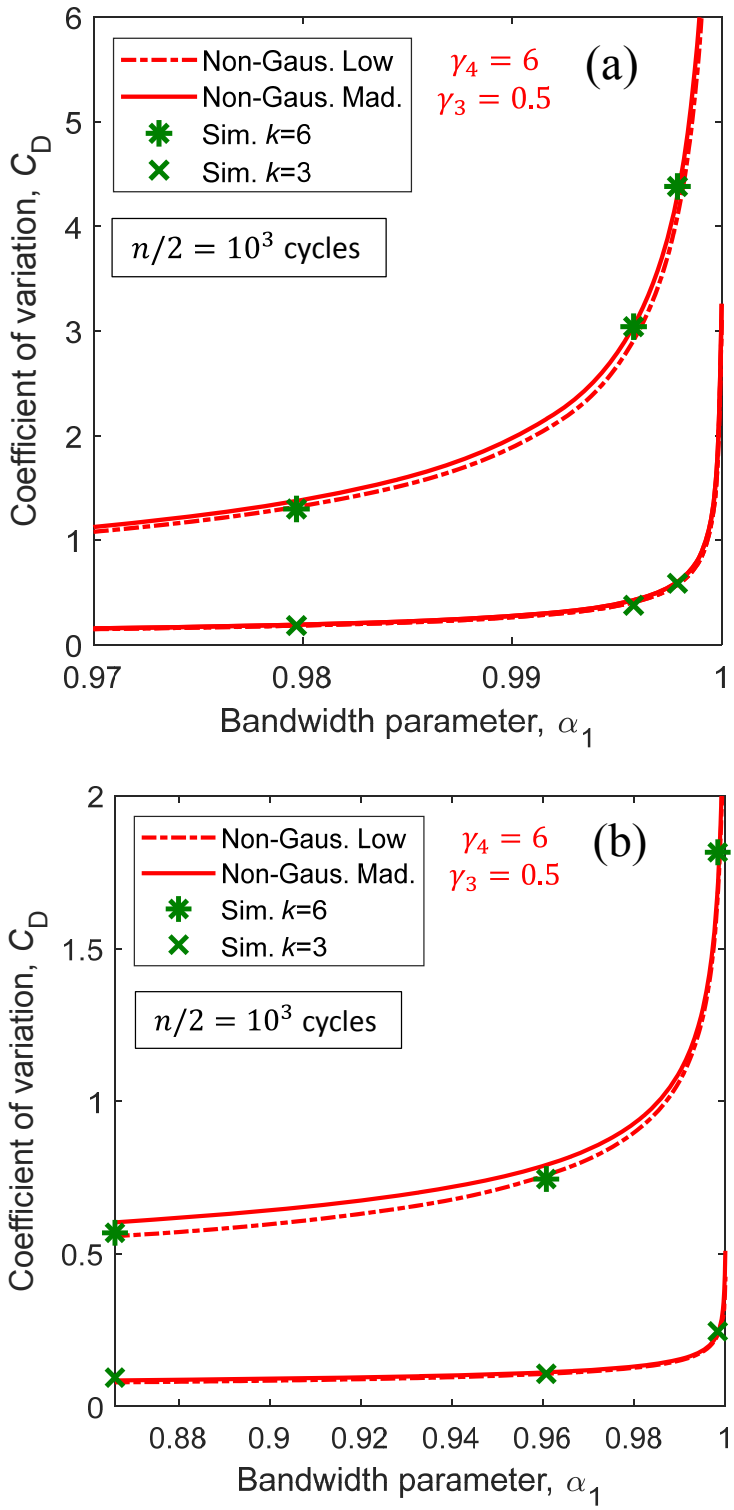

Figure 7. Trends of the CoV as a function of the bandwidth parameter α_1, for (a) linear oscillator and (b) ideal unimodal PSD. Solid lines are the theoretical estimations, markers come from time-domain simulations.

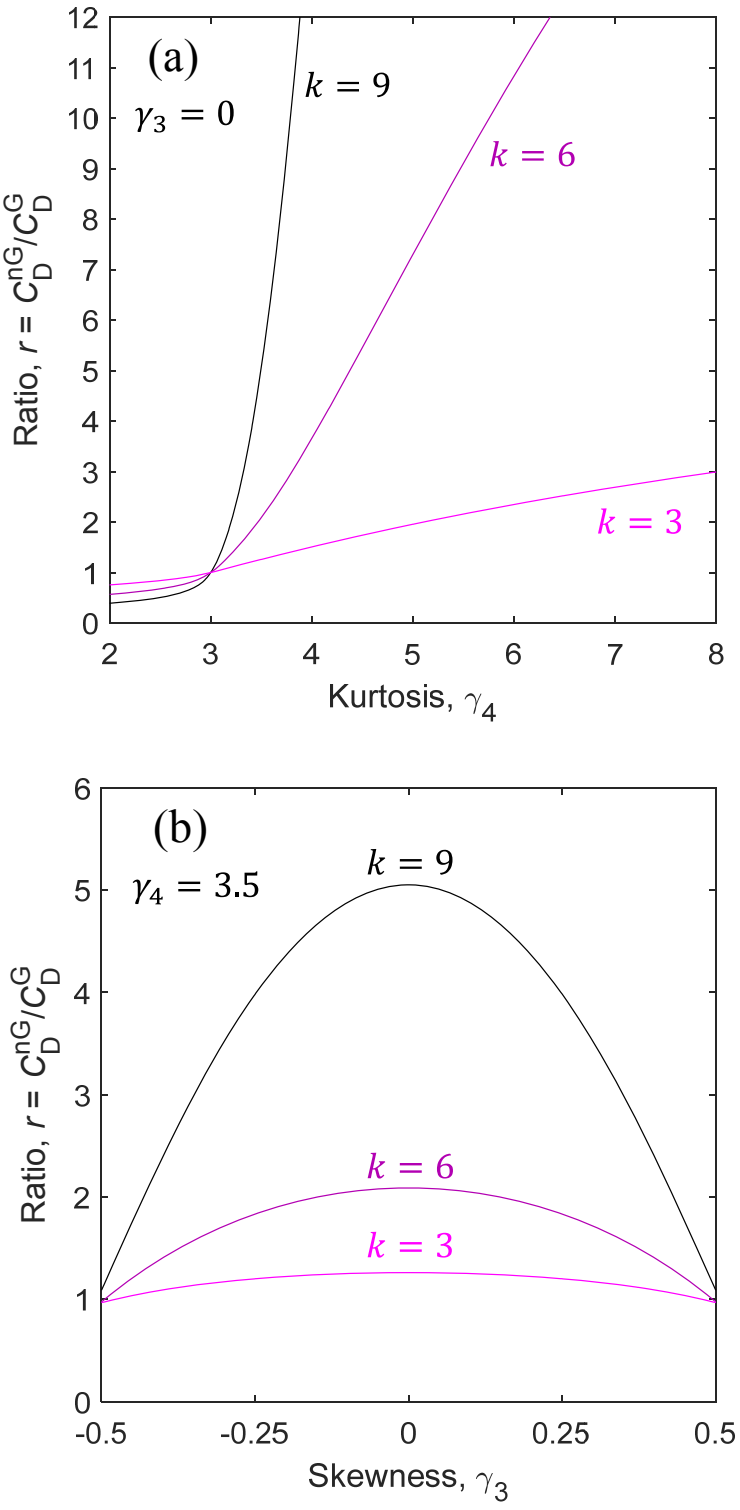

Figure 8. Ratio of coefficient of variation of damage $r = (C_D)^{nG}_{\text{Mad}}/(C_D)^{G}_{\text{Mad}}$ versus (a) kurtosis coefficient and (b) skewness coefficient, for several values of the inverse slope k of the S-N curve.

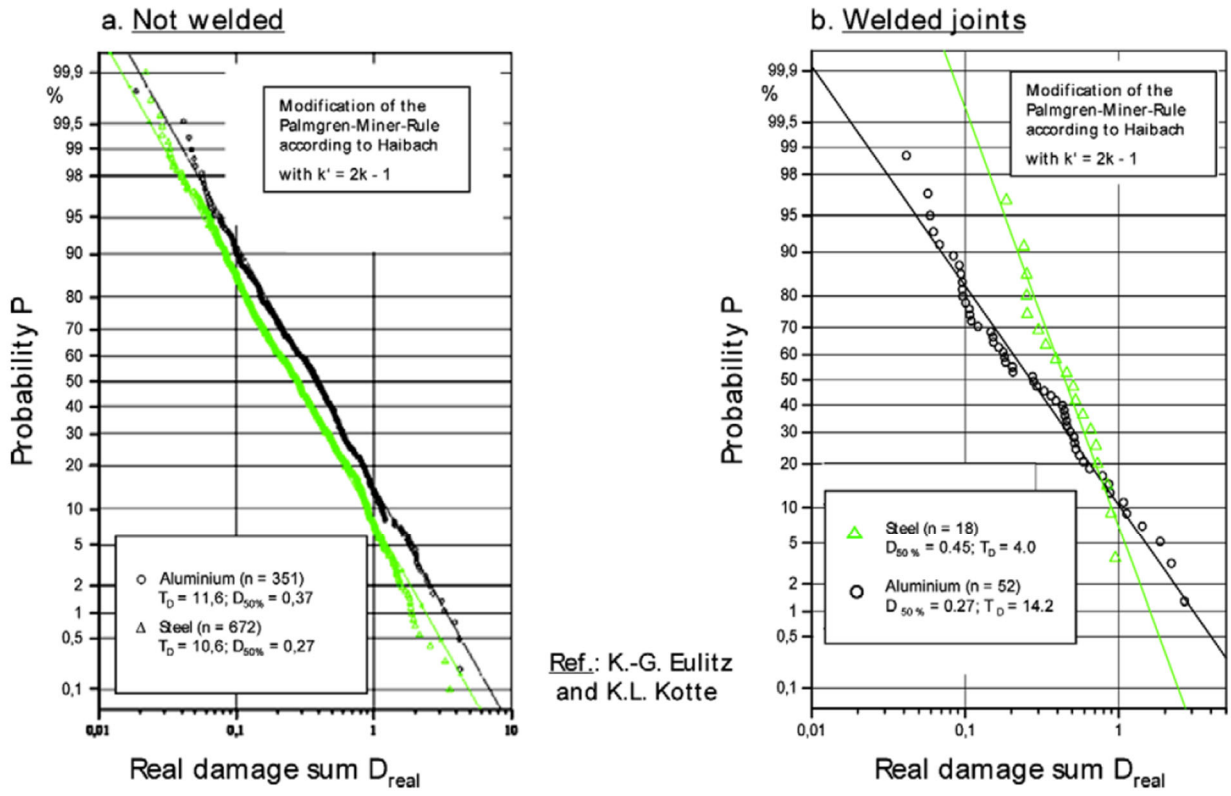

Figure 9. Statistical distribution of the real damage sum (critical damage) for steel and aluminium. (Reprinted from Sonsino CM Int J Fatigue 2007;29:1080-1089, with permission from Elsevier)

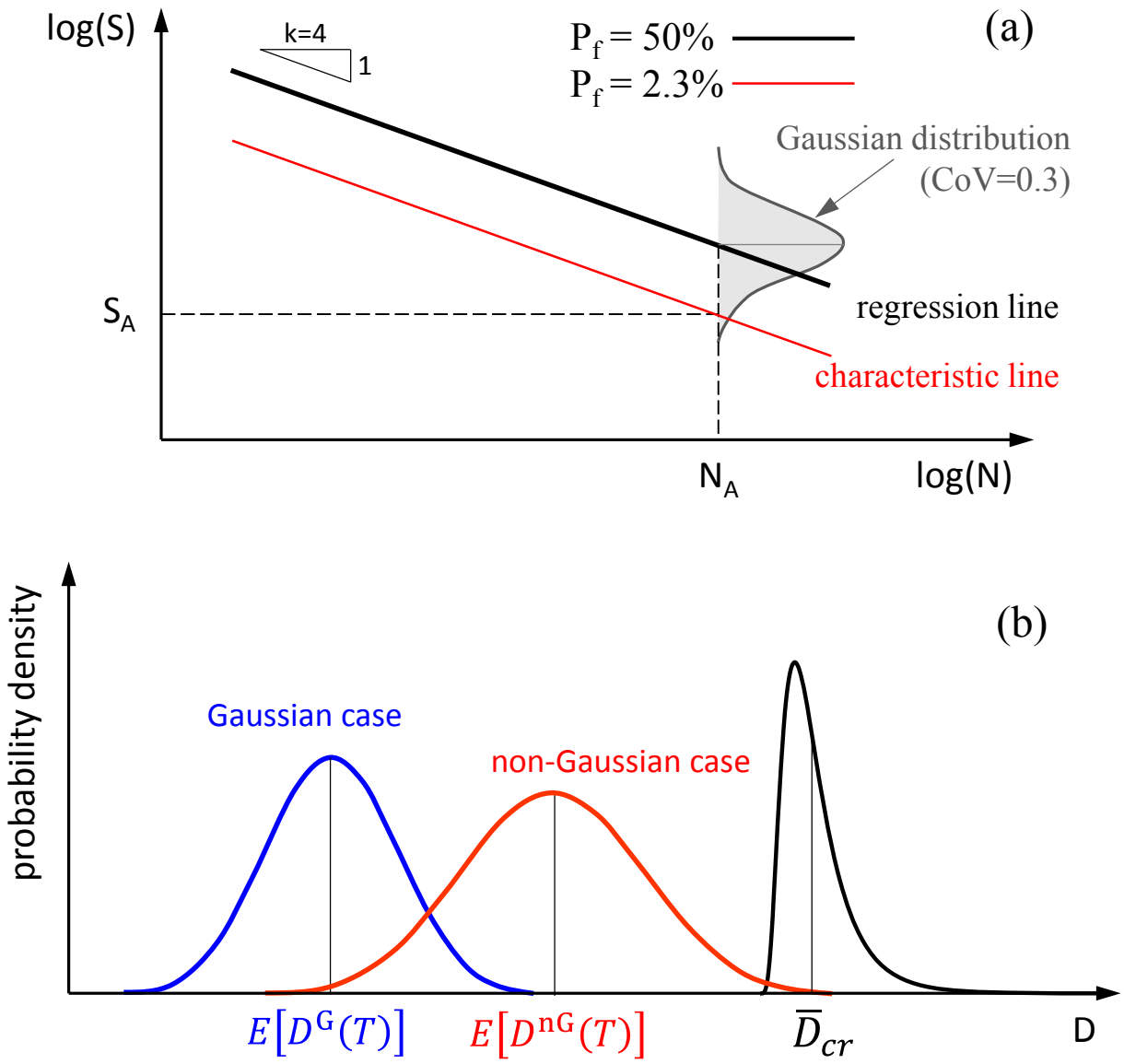

Figure 10. (a) Characteristic S-N line including the variability of fatigue strength; (b) probability distributions involved in the computation of the failure probability.

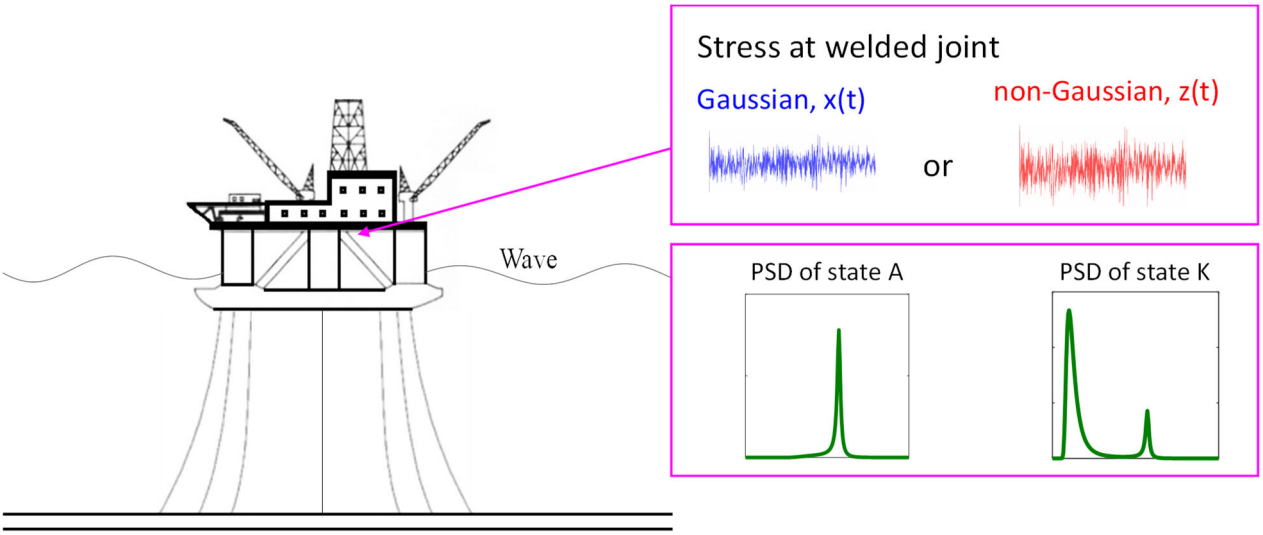

Figure 11. Offshore platform under wave loading, with a Gaussian or non-Gaussian time-history acting on a critical welded joint.

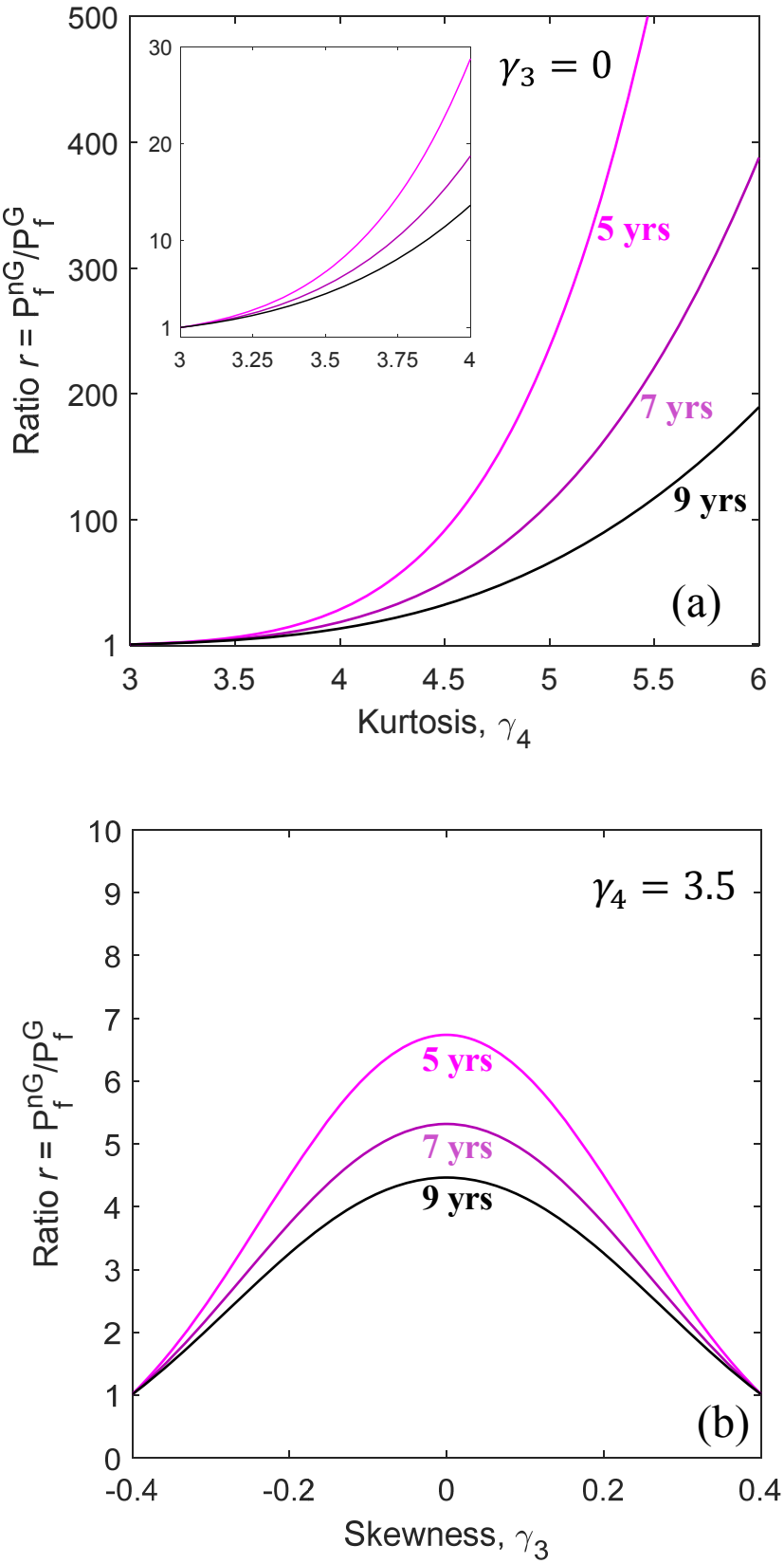

Figure 12. Increment of the failure probability due to a non-Gaussian time-history with: (a) skewness $\gamma_3 = 0$ and kurtosis γ_4 from 3 to 6; (b) kurtosis $\gamma_4 = 3.5$ and skewness from -0.4 to 0.4.